

NAVAL POSTGRADUATE SCHOOL

Monterey, California

AD-A205 692



THESIS

**THE EFFECT OF WELDING PROCESS
ON THE MICROSTRUCTURE OF
HY-130 STEEL WELDMENTS**

by

Teresa M. McNutt

December 1988

Thesis Co-Advisors:

J. Mauro Losz
Saeed Saboury

Approved for public release; distribution is unlimited.

DTIC
ELECTE
MAR 28 1989
S H D

89 3 27 072

Unclassified

Security Classification of this page

REPORT DOCUMENTATION PAGE

| | | | | | |
|---|-------|--|--|---|---------------------------|
| 1a Report Security Classification Unclassified | | | 1b Restrictive Markings | | |
| 2a Security Classification Authority | | | 3 Distribution Availability of Report | | |
| 2b Declassification/Downgrading Schedule | | | Approved for public release; distribution is unlimited. | | |
| 4 Performing Organization Report Number(s) | | | 5 Monitoring Organization Report Number(s) | | |
| 6a Name of Performing Organization Naval Postgraduate School | | 6b Office Symbol (If Applicable) 69 | 7a Name of Monitoring Organization Naval Postgraduate School | | |
| 6c Address (city, state, and ZIP code) Monterey, CA 93943-5000 | | | 7b Address (city, state, and ZIP code) Monterey, CA 93943-5000 | | |
| 8a Name of Funding/Sponsoring Organization | | 8b Office Symbol (If Applicable) | 9 Procurement Instrument Identification Number | | |
| 8c Address (city, state, and ZIP code) | | | 10 Source of Funding Numbers | | |
| | | | Program Element Number | Project No | Task No |
| | | | Work Unit Accession No | | |
| 11 Title (Include Security Classification) The Effect of Welding Process on the Microstructure of HY-130 Steel Weldments | | | | | |
| 12 Personal Author(s) Teresa Marie McNutt | | | | | |
| 13a Type of Report Master's Thesis | | 13b Time Covered From To | | 14 Date of Report (year, month, day) December 1988 | |
| 15 Page Count 76 | | | | | |
| 16 Supplementary Notation The views expressed in this thesis are those of the author and do not reflect the official policy or position of the Department of Defense or the U.S. Government. | | | | | |
| 17 Cosati Codes | | | 18 Subject Terms (continue on reverse if necessary and identify by block number) | | |
| Field | Group | Subgroup | HY-130 Steel, GMAW, SAW, Welding Microstructure | | |
| | | | | | |
| | | | | | |
| 19 Abstract (continue on reverse if necessary and identify by block number) | | | | | |
| <p>HY-130 is a high-strength, low-carbon steel used in the quenched and tempered condition. It is designed for high performance and marine applications where good weldability is a requirement. Optimum welding parameters are currently under investigation. In this study, 1/2 inch (12.7 mm) HY-130 steel weldments produced by submerged arc welding (SAW) and gas metal arc welding (GMAW) processes are compared by means of a systematic microstructural characterization of the base metal, weld metal, and heat affected zone (HAZ). The microstructures are characterized by optical and electron microscopy and microhardness measurements are performed in the weld metal and across the HAZ to relate the microstructure with the microhardness profiles. The weld metal microstructure of both weldments showed a predominantly martensitic structure. The GMAW weld metal had a finer lath martensite structure and contained more retained austenite and twinned martensite. The SAW weld metal had a less defined lath structure which was more bainitic. The microhardness values were higher in the GMAW weld metal. No significant differences in microstructure and hardness were observed in the HAZ of the two weldments.</p> | | | | | |
| 20 Distribution/Availability of Abstract | | | 21 Abstract Security Classification | | |
| <input checked="" type="checkbox"/> unclassified/unlimited <input type="checkbox"/> same as report <input type="checkbox"/> DTIC users | | | Unclassified | | |
| 22a Name of Responsible Individual Professor S. Saboury | | | 22b Telephone (Include Area code) (408) 646-2656 | | 22c Office Symbol 69Ss |

DD FORM 1473, 84 MAR

83 APR edition may be used until exhausted

security classification of this page

All other editions are obsolete

Unclassified

Approved for public release; distribution is unlimited.

**The Effect of Welding Process on the
Microstructure of HY-130 Steel Weldments**

by

Teresa M. McNutt
Captain, Canadian Forces
B.Sc. (Chem. Eng.), Queen's University at Kingston, Canada, 1983

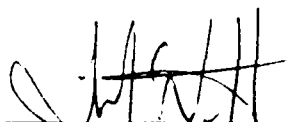
Submitted in partial fulfillment of the
requirements for the degree of

MASTER OF SCIENCE IN MECHANICAL ENGINEERING

from the

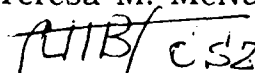
NAVAL POSTGRADUATE SCHOOL
December 1988

Author:

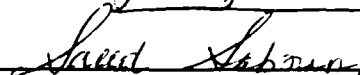


Teresa M. McNutt

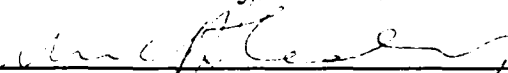
Approved by:



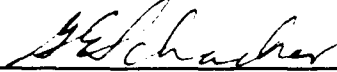
J. Mauro Losz, Thesis Co-Advisor



Saeed Saboury, Thesis/Co-Advisor



A. J. Healey, Chairman,
Department of Mechanical Engineering



Gordon E. Schacher, Dean of
Science and Engineering

ABSTRACT

HY-130 is a high-strength, low-carbon steel used in the quenched and tempered condition. It is designed for high performance and marine applications where good weldability is a requirement. Optimum welding parameters are currently under investigation. In this study, 1/2 inch (12.7 mm) HY-130 steel weldments produced by submerged arc welding (SAW) and gas metal arc welding (GMAW) processes are compared by means of a systematic microstructural characterization of the base metal, weld metal, and heat affected zone (HAZ). The microstructures are characterized by optical and electron microscopy and microhardness measurements are performed in the weld metal and across the HAZ to relate the microstructure with the microhardness profiles. The weld metal microstructure of both weldments showed a predominantly martensitic structure. The GMAW weld metal had a finer lath martensite structure and contained more retained austenite and twinned martensite. The SAW weld metal had a less defined lath structure which was more bainitic. The microhardness values were higher in the GMAW weld metal. No significant differences in microstructure and hardness were observed in the HAZ of the two weldments.

iii



| | |
|--------------------|--|
| Accession For | |
| NTIS GRA&I | <input checked="checked" type="checkbox"/> |
| DTIC TAB | <input type="checkbox"/> |
| Unannounced | <input type="checkbox"/> |
| Justification | |
| By | |
| Distribution/ | |
| Availability Codes | |
| Dist | Avail and/or Special |
| A-1 | |

TABLE OF CONTENTS

| | |
|--|-----------|
| I. INTRODUCTION..... | 1 |
| II. BACKGROUND | 3 |
| A HY-130 STEEL..... | 3 |
| B MICROSTRUCTURE | 4 |
| C WELDING PROCESSES | 6 |
| D COOLING RATE..... | 8 |
| E INCLUSIONS..... | 13 |
| III. EXPERIMENTAL PROCEDURE..... | 16 |
| A MATERIAL AND MATERIAL PREPARATION | 16 |
| B MICROHARDNESS TRAVERSES | 18 |
| C MICROSTRUCTURAL CHARACTERIZATION | 19 |
| IV. RESULTS | 22 |
| A MACROSTRUCTURE | 22 |
| B MICROHARDNESS MEASUREMENTS..... | 26 |
| C MICROSTRUCTURAL CHARACTERIZATION | 32 |
| 1. Optical Microscopy..... | 33 |
| 2. Scanning Electron Microscopy (SEM)..... | 33 |

| | |
|--|-----------|
| 3. Transmission Electron Microscopy (TEM)..... | 38 |
| a. Base Metal..... | 38 |
| b. Weld Metal of the Last Pass..... | 54 |
| c. Weld Metal Close to Coarse HAZ..... | 55 |
| d. Coarse HAZ..... | 56 |
| e. Fine HAZ..... | 56 |
| V. DISCUSSION..... | 58 |
| VI. SUMMARY | 64 |
| LIST OF REFERENCES..... | 65 |
| INITIAL DISTRIBUTION LIST..... | 68 |

ACKNOWLEDGMENTS

I wish to express my appreciation to my thesis advisors, Dr. J. Mauro Losz and Dr. Saeed Saboury. I thank Mauro for his transmission electron microscopy and photographic instruction and Saeed for his guidance, concern, and unending dedication.

I extend a very special thank you to Claudine Guerin and Robert Perron for their love and attention which they generously shared with my two daughters while I was completing my studies. Also, I thank my parents, Garth and Veronica Cornwall and Joyce and Reg McNutt, for their support and assistance when each of our daughters was born.

I express my appreciation to the Canadian Forces and particularly to my branch for offering such a superb educational opportunity to my husband and me.

Finally, to my husband, Steven, and daughters, Kaitlyn and Megan, I apologize for not spending as much time with you as I would have liked. I dedicate this work to the three of you.

I. INTRODUCTION

HY-130 steel is a low-carbon, 130 ksi yield-strength, high-toughness alloy steel designed for high-performance applications. The advantages of the HY steels are their good combination of strength and toughness over a large temperature range and their good weldability with little or no post-weld heat treatment [Ref. 1]. HY-130 steel achieves its strength and toughness through a quench and temper heat treatment.

The United States Navy has sponsored the development of the HY-130 system as a replacement for the lower-strength HY-80 system in the construction of submarine hulls. The HY-130 steel system under development includes specifications for rolled plate; forged, extruded, and cast product forms; and required filler metal and welding procedures for the fabrication of high-strength and high-toughness structures [Ref. 2]. HY-130 steel can provide a deeper operating depth capability for submersibles and an increased strength-to-weight ratio. HY-130 steel is currently used by the U.S. Navy for submersibles and is a candidate for use in the SSN-21 submarine design for nonpressure hull structures [Ref. 3]. The use of HY-130 steel is estimated to provide a weight savings of 40 to 50 tons over HY-100 steel in the SSN-21 submarine [Ref. 3]. The high cost of labor-intensive welding and the great potential for weight reduction have motivated research to identify the optimum welding parameters for HY-130 steel.

This thesis provides a microstructural comparison of the gas-metal-arc welding (GMAW) and submerged-arc welding (SAW) processes on one-inch (25.4 mm) thick plates of HY-130 steel. Microstructural characterization of the weld metal and heat-affected zones is presented based on analyses made through microhardness testing and optical, scanning, and transmission electron microscopy.

II. BACKGROUND

A. HY-130 STEEL

HY-130 steel is a hardenable high-strength steel developed for high-performance and marine applications. It is used in the quenched and tempered condition and has good weldability. The carbon content is maintained at less than 12 weight percent and it is a medium alloy-type steel.

The roles of the key elements of HY-130 steel are described in Reference 2. In summary:

| | |
|---------------|---|
| C | is kept low (between 0.08 and 0.12 weight percent) to ensure good notch toughness and weldability; |
| Ni | lowers the transformation temperature and contributes to solid solution strengthening; |
| Cr, Mo, and V | are strong carbide formers, improve hardenability, but are kept low to reduce embrittlement; |
| Mn | increases hardenability but is kept below 0.09 percent to avoid poor toughness; |
| Si | controls the occurrence of oxidation and maintains a low transition temperature and satisfactory notch toughness; |
| P | is kept low to reduce embrittlement; |
| Al | improves toughness without the formation of aluminum nitride precipitates; and |
| H | is kept as low as possible to prevent hydrogen embrittlement. |

HY-130 steel is produced with a high degree of cleanliness, so sulfur and oxygen are kept to the lowest possible levels.

HY-130 is used in the quenched and tempered condition and requires a minimum of 60 to 75 percent martensite [Ref. 2] with a maximum of 40 percent lower bainite at the center of a four-inch plate [Ref. 1]. The austenitizing temperature is recommended as 1,500° F. (815.6° C) with a tempering range of 1,000° to 1,150° F (537.8° to 621.1° C) followed by a water quench. These temperatures are lower than for the HY-80 steels, in which the austenitizing temperature is recommended as 1,650° F (898.9° C) with a tempering range of 1,150° to 1,250° F (621.1° to 676.7° C). [Ref. 1]

B. MICROSTRUCTURE

The microstructure development of low-carbon weldments has been studied by several authors. The transformation sequence is summarized in References 4, 5, and 6 and is outlined here.

Below the austenitizing temperature, ferrite initially nucleates at austenite grain corners and along the boundaries as these sites usually provide the lowest energy barrier. The ferrite growth is planar and leads to the formation of grain boundary alliotriomorphs or blocky ferrite. Subsequently, sideplates develop from the grain boundary ferrite and grow very rapidly. Often this results in parallel arrays of ferrite laths adjacent to the prior austenite grain boundaries. Occasionally, large polygonal ferrite grains are observed in this region. Acicular ferrite may start to nucleate intragranularly at inclusions. This heterogeneous nucleation may also occur at twin boundaries or stacking faults in the austenite or at pre-existing Widmanstatten ferrite. Acicular ferrite is a fine-grained Widmanstatten type of ferrite, nucleated in the

transformation temperature range between grain boundary ferrite and upper bainite. The acicular ferrite laths grow until impingement occurs on neighboring grains and the final lath size is determined by the average spacing between inclusions. The typical width of individual laths is one to three μm [Ref. 4]. If acicular ferrite formation is suppressed due to a lack of nucleation sites, ferrite side plates and bainite microstructures will dominate.

As ferrite forms during cooling, the remaining austenite is continuously enriched with carbon. This austenite may decompose to a variety of microstructural constituents, including pearlite, upper and lower bainite, or martensite, depending on the cooling rate and composition.

In Fe-C alloys, the parent phase, austenite, may transform to martensite on rapid cooling. The martensite has the exact same composition as the austenite (up to two percent carbon), as the transformation is diffusionless. Two morphologies of martensite develop in heat-treatable carbon steels, lath and plate. Lath martensite forms in low-and medium-carbon steels, while plate martensite forms in high-carbon steel. Laths of martensite tend to align themselves parallel to one another, separated by low-angle grain boundaries. These regions of parallel lath alignments are referred to as packets. Most laths have widths smaller than $0.5\ \mu\text{m}$ but may be as wide as $2.0\ \mu\text{m}$. The fine structure of lath martensite consists of a very high dislocation density estimated at 10^{12} dislocations per square centimeter. Fine transformation twins also may be formed, to a much lesser extent, in Fe-C lath

martensite. The amount of fine twinning increases with decreasing martensite transformation temperature (M_s) as the carbon content increases. [Ref. 6]

Bainite forms under continuous cooling rates intermediate to those of pearlite and martensite formation. Bainite consists of fine aggregates of ferrite and cementite. The ferrite in bainite may be lath or plate-like containing a dislocation substructure. Two morphologies of bainite exist, upper and lower bainite. Upper bainite forms in the temperature range just below that of pearlite, while lower bainite forms at temperatures closer to the M_s . The carbide particles of upper bainite tend to be elongated and form between ferrite laths. In some steels, especially those with high silicon content, the carbon-enriched austenite between the bainite laths is quite stable and is retained between the ferrite laths at room temperature. Lower bainite is composed of relatively large plates and is often characterized as acicular. Fine carbides form within the plates, which is in contrast with upper bainite, where coarser carbides form between the plates. [Ref. 6]

Thompson, et al. [Ref. 7] have identified a granular bainite, in low-carbon, copper-bearing steels such as A710, which is described as laths of ferrite which have a very similar crystallographic orientation within each packet and interlath particles of martensite and/or austenite.

C. WELDING PROCESSES

Fusion welding is the most important technique used in welding construction today [Ref. 8]. The two fusion-welding processes used in

this study were submerged-arc welding (SAW) and gas-metal-arc welding (GMAW).

SAW involves an automatically fed, continuous electrode wire and a separate granular flux. The flux is usually delivered slightly ahead of the welding electrode. The arc is initiated between the electrode and the workpiece and is insulated by the flux, preventing atmospheric contamination and rapid dissipation of heat. This results in relatively high welding speeds and deep penetration. The melted flux reacts with the weld pool and adds certain alloying elements to the weld metal. For HY-130 weldments, the filler metal selection is made such that the as-deposited weld metal will possess similar properties as the fully heat-treated base metal. Large heat-affected zones (HAZs) are characteristic of SAW as approximately two volumes of base metal are melted for each volume of filler metal [Ref. 9]. SAW is a high production process known for its high deposition rates. It is, however, limited to flat and horizontal positions to avoid flux run-off. [Ref. 10]

The GMAW process uses an electric arc between a consumable wire electrode and the workpiece. A gas shields the arc and weld pool from the atmosphere, preventing oxidation and contamination. GMAW is often performed with DC reverse polarity (DCRP), which results in a more stable transfer and deeper penetration than DC straight polarity (DCSP). The GMAW process has high productivity, reliability, and all-position capability. [Ref. 10]

Figure 1 shows the different sub-zones of a weld. Multi-pass welds result in refinements in microstructure, improvements in toughness, and reductions in residual stresses as compared to single-run welds [Ref. 8]. Each subsequent weld thermal cycle refines the grains of the underlying portion of the previous weld metal. Figure 2 is a schematic showing the resulting microstructures of single- and multi-run welds. Challenger, et al. [Ref. 11] used TEM to show that overlapping the weld beads is necessary in GMAW of HY-130 to produce a microstructure with the required yield strength. If overlapping is not employed, there is little tempering of the martensite, resulting in less fracture resistance.

D. COOLING RATE

The weld metal microstructure is a function of the cooling rate (or heat input rate) and composition. Higher cooling rates are associated with lower heat input rates. Cooling is continuous, therefore continuous cooling transformation (CCT) diagrams may be used to predict the microstructure of the particular weld metal composition. A schematic CCT diagram for low-carbon steel [Ref. 12] is included at Figure 3. This summarizes the weld metal microstructure expected as a function of cooling rate. The cooling rate determines the extent of supercooling prior to the transformation of austenite, which affects the driving force for the reaction. From the CCT diagram it is seen that increasing the cooling rate would increase the formation of acicular ferrite or upper bainite, hence it is a mechanism of microstructural refinement.

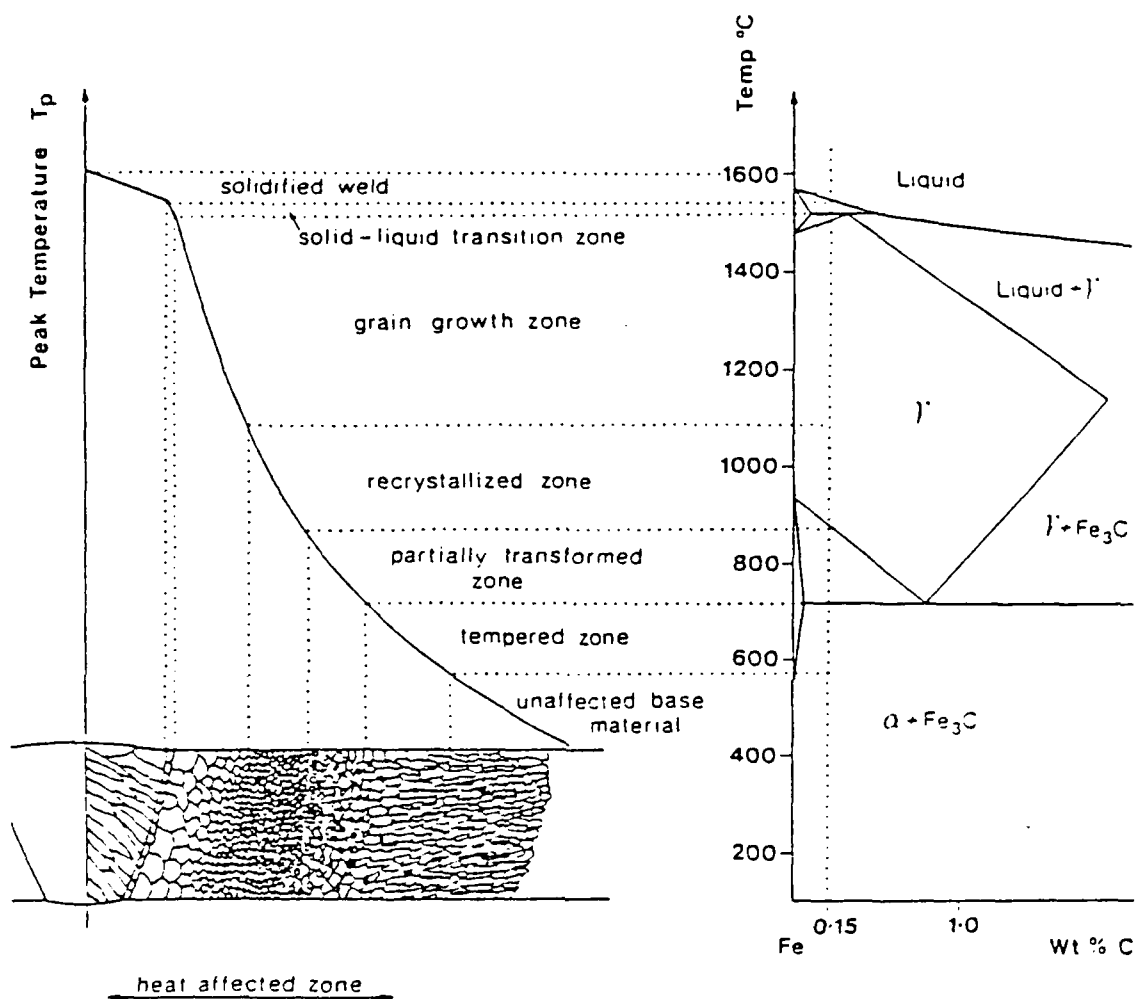


Figure 1. Schematic Diagram of the Various Sub-Zones of the Heat-Affected Zone Approximately Corresponding to a 0.15 Weight Percent C Alloy Indicated on the Fe-Fe₃C Equilibrium Diagram [Ref. 8]

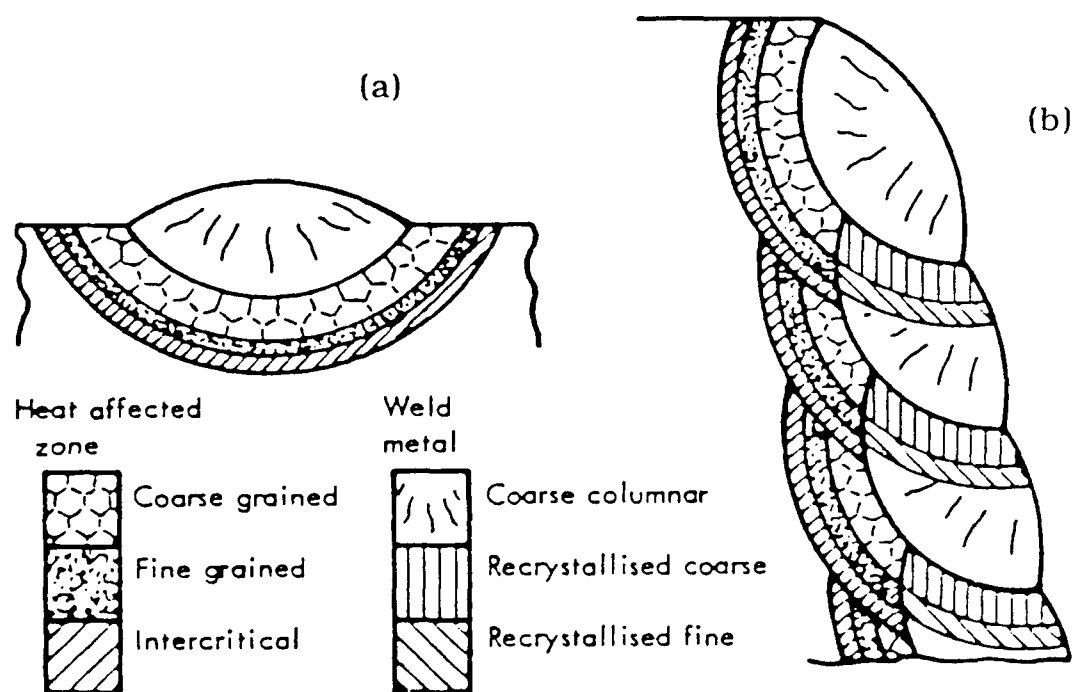


Figure 2. Schematic Comparison of the Microstructures of
(a) Single-Run and (b) Multi-Run Welds [Ref. 8]

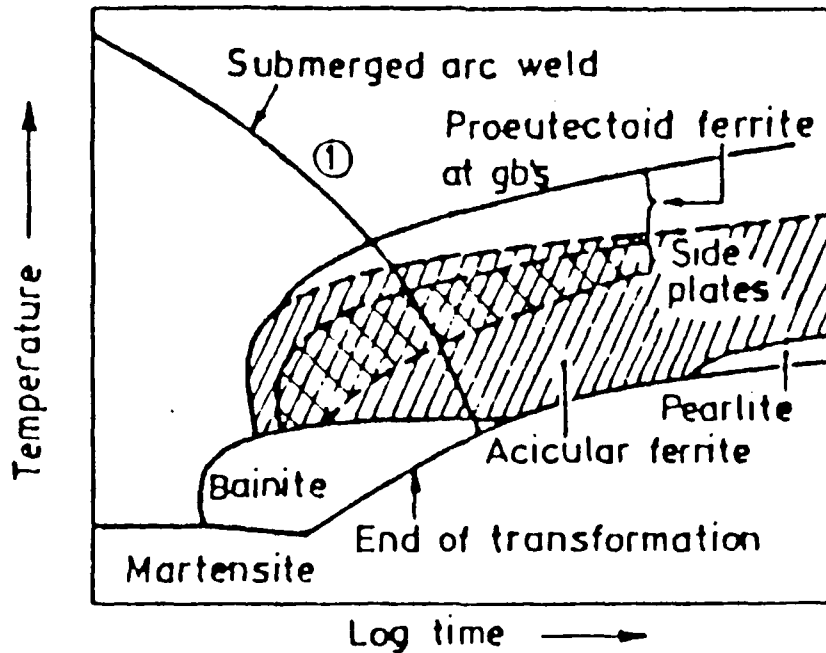


Figure 3. Schematic CCT Diagram for Weld Metal of 0.17 Percent C-1.39 percent Mn Steel with Approximately 0.03 Percent Oxygen [Ref. 12]

The overall effect of increasing the cooling rate is to lower the transformation temperature. Harrison observed that at low cooling rates (less than $1\text{ }^{\circ}\text{C/s}$ for the $800\text{--}500^{\circ}\text{C}$ range), polygonal ferrite and pearlite were the dominant transformation products. The polygonal ferrite is refined as the cooling rate is increased and becomes confined to the prior austenite grain boundaries. Widmanstätten side plates also developed from the interface of the polygonal phase. At intermediate cooling rates ($15\text{ }^{\circ}\text{C/s}$), intragranular products, including acicular and coarse acicular ferrite, developed. At higher cooling rates (above 200°C/s), parallel laths of ferrite surrounded by retained austenite, martensite-austenite (M-A), or carbides were present. A

martensitic transformation replaced the lath structure when high basic hardenability was also present. [Ref. 13]

Using the SAW process, Glover, et al. found that as the heat input increased from 0.74 kJ/mm to 10 kJ/mm, the weld metal of a C-Mn steel (C above 0.13 percent, about 1.1 percent Mn, 0.25 percent Si, 0.2 percent Mo, and 0.035 Nb) changed from martensite to upper bainite to acicular ferrite. An M-A microconstituent located between the ferrite laths was replaced by carbides as the heat input increased. In low-carbon, high-strength, low-alloy (HSLA) steels (C below 0.07 percent), the weld metal changed from coarse polygonal ferrite to acicular ferrite to upper bainite. A blocky or elongated M-A microconstituent was formed in the cooling range 15s to 190s while no distinct carbide formed. [Ref. 14]

Wong reported that longitudinal flat two-inch (51 mm) gage tensile specimens of HY-130 exhibited an increased yield strength with increases in cooling rate. Hardness measurements taken at the center of the weld decreased only slightly with increased heat input. For heat inputs ranging from 20 kJ/in to 41 kJ/in (0.79 to 1.6 kJ/mm), the Rockwell C hardness measurements were 36 to 34, respectively. [Ref. 3]

The cooling rate strongly influences the transformation kinetics as well as the mechanical properties of the weld metal. A minimum cooling rate for 25 to 50 mm HY-130 steel plates has been specified as 30 F°/second at 1,000° F or 16.7 C°/s at 537.8° C [Ref. 1], which limits the maximum allowable preheat temperature. Lower cooling rates will

result in weld metal yield strengths below 130 ksi. Wong reported that a minimum cooling rate of 35 F°/s at 1,000° F (19.4 C°/s at 537.8° C) for 1/2 inch (12.7 mm) plates was required to produce adequate mechanical properties in longitudinal weld metal of HY-130 steel. For GMAW processes, he found that a heat input of 30 to 35 kJ/in (1.18 to 1.38 kJ/mm) should be used with 1/2 inch (12.7 mm) plates. Extrapolation showed that a 40 kJ/in (1.57 kJ/mm) heat input should be limited to 3/4 inch (19 mm) plates or greater. Flax, et al. [Ref. 1] state the recommended input energy as 45 kJ/in (1.77 kJ/mm) for GMAW with a limit of 50 kJ/in (1.97 kJ/mm) for a one-inch (25.4 mm) plate. Flax also reports the minimum preheat and interpass temperature for one-inch (25.4 mm) plate HY-130 steel as 200° F (93.3° C). The maximum preheat temperature is listed as 300° F (148.9° C) or as high as 400° F (204.4° C) to avoid transverse cracking in the weld metal.

E. INCLUSIONS

Many authors state that inclusions play an important role in phase transformations by providing suitable nucleation sites for acicular ferrite. Bhatti, et al. [Ref. 15] found that the controlling factors in determining the effectiveness of inclusions as nucleants in SAW of API 5LX65 steel (0.052 percent C, 1.37 percent Mn, 0.224 percent Si, 0.34 Cu) are volume fraction and size distribution. It is debated whether it is the inclusion crystallography or the indirect effect of inclusion chemistry on hardenability that is of importance in the nucleation of acicular ferrite. It seems that a threshold value of 1.1

percent Mn must be exceeded in the weld metal for acicular ferrite to develop [Ref. 15].

Bhatti, et al. also found that inclusions are generally globular in shape in the weld metal. They were, however, accompanied by distinctly geometrical inclusions in the beads when high basicity flux was used. These inclusions were triangular, rectangular, pentagonal, and hexagonal in shape and very rich in Al. The Al-rich inclusions were accompanied by a larger amount of acicular ferrite than the Mn-rich inclusions which had a lesser amount of acicular ferrite.

Lui and Olson [Ref. 16] studied the effect of inclusions in the weld metal of SAW HSLA steel. They found that the inclusion volume fraction can be directly related to the concentration of inclusion formers (oxygen and sulfur) and affects the austenite to ferrite transformation. They related the microstructure to weld metal oxygen content and found that the mean particle size of weld metal inclusions decreased with increasing concentration of oxygen. The inclusion size distribution dictated whether the oxide and oxy-sulfide inclusions were located largely at austenite grain boundaries or intragranularly, which controlled the final weld metal microstructure. Particles with diameters smaller than a critical size were often found at the boundaries and were effective at pinning the austenite grain boundary. Since grain boundary nucleation of ferrite is quite favorable, site saturation occurs quickly, followed by allotriomorphic growth. Weld metals with high oxygen content and a large amount of grain boundary ferrite were associated with a large number of small-size inclusions of diameters of

less than one μm and with fine austenite grains. Intragranular inclusions provided the initial nucleation sites for acicular ferrite formation. A higher acicular ferrite content was associated with a large number of inclusions of diameter greater than two μm and with coarser austenite grains, resulting in a refined microstructure. The larger austenite grains result in a smaller grain boundary surface area, reducing the availability of grain boundary nucleation sites, hence the amount of grain boundary ferrite is reduced.

Ricks, et al. [Ref. 17] studied the influence of second-phase particles and concluded that inert, nondeformable inclusions are always less-effective sites for nucleation than grain boundaries. Only after site saturation of the boundaries had taken place could nucleation on inclusions occur. It has also been noted by several authors that inclusions can accelerate nucleation through the thermal expansion difference between the inclusion and the matrix [Ref. 16]. The austenite matrix is strained at inclusion locations, during cooling, which accelerates its transformation into ferrite.

III. EXPERIMENTAL PROCEDURE

A. MATERIAL AND MATERIAL PREPARATION

Two HY-130 steel plates about 25 mm thick with the chemical composition given in Table I were welded by multi-pass gas-metal-arc (GMAW) and submerged-arc (SAW) welding processes. The weld preparation for each plate was a single beveled, 60° V-joint with a backing plate tack-welded at the base of each plate at the joint. Both welds were made using identical electrode material of the chemical composition listed in Table I. The welding parameters of each process are summarized in Table II. Each plate measured one inch (25.4 mm) long in the welding direction. The weldments were fabricated by David Taylor Naval Ship Research and Development Center (DTNSRDC), Annapolis, Maryland, and were sent to the Naval Postgraduate School for examination.

The plates were sectioned perpendicular to the weld into approximately one-half inch (12.7 mm) thick specimens. Each specimen face was sanded to produce a smooth, flat surface suitable for macroetching. The samples were then etched in a two-percent Nital solution for about ten minutes until details of each weld pass became clear.

Rockwell C hardness measurements were taken in the base metal.

TABLE I

**CHEMICAL COMPOSITION OF HY-130 BASE PLATE,
WELD METAL, AND FILLER METAL**

| Element | Base Plate | Weld Metal GMAW | Weld Metal SAW | Filler Metal* |
|----------------|-------------------|----------------------------|---------------------------|----------------------|
| Carbon | 0.106 | 0.074 | 0.055 | 0.091 |
| Manganese | 0.87 | 1.46 | 1.44 | 1.67 |
| Silicon | 0.22 | 0.30 | 0.37 | 0.39 |
| Phosphorus | 0.007 | 0.006 | 0.014 | 0.005 |
| Sulfur | 0.002 | 0.005 | 0.001 | 0.010 |
| Nickel | 4.40 | 2.39 | 2.40 | 2.23 |
| Molybdenum | 0.42 | 0.62 | 0.62 | 0.63 |
| Chromium | 0.51 | 1.05 | 0.99 | 1.05 |
| Vanadium | 0.058 | 0.014 | 0.020 | 0.011 |
| Aluminum | 0.019 | 0.003 | 0.014 | 0.004 |
| Titanium | 0.002 | 0.003 | 0.004 | 0.010 |
| Zirconium | 0.001 | 0.001 | 0.001 | 0.003 |
| Copper | 0.057 | 0.046 | 0.046 | 0.045 |
| Oxygen | 0.0060 | 0.019 | 0.028 | 0.0030 |
| Nitrogen | 0.008 | 0.0046 | 0.005 | 0.0030 |
| Boron | 0.004 | 0.005 | 0.003 | 0.004 |
| Arsenic | - | - | - | 0.011 |
| Hydrogen | 1.4 ppm | 1.4 ppm | 0.4 ppm | 0.0002 |

*The filler metal also contains small amounts of lead, bismuth, tin, antimony, niobium, calcium, cerium, and yttrium.

TABLE II

WELDING PARAMETERS FOR SAW AND GMAW WELDMENTS

| Welding Process | SAW | GMAW |
|--------------------------------------|--------------------------|--------------------------|
| Weld ID Number | F258 | F262 |
| Thickness | 1 inch 25.4 mm | 1 inch 25.4 mm |
| Number of Passes | 40 | 21 |
| Current (amp) | 300 | 340 |
| Voltage (kV) | 34 | 27 |
| Polarity | DCRP | DCRP |
| Travel Speed | 17.5 in/min 7.41 mm/s | 11 in/min 4.66 mm/s |
| Heat Input | 35.0 kJ/in 1.38 kJ/mm | 50.1 kJ/in 1.97 kJ/mm |
| Preheat/Interpass Temperature | 200° F 93.3° C | 250° F 121.1° C |
| Cooling Rate at 1,000° F or 537.8° C | 34 F° 18.9 C° | 38 F° 21.1 C° |

B. MICROHARDNESS TRAVERSES

Samples were cut from the macrosamples, metallographically mounted, polished, and etched in two-percent Nital to locate regions for analyses. To facilitate microhardness measurements, a line was scribed across each selected region with a diamond scribe. The samples were then lightly polished in order to remove the etch and subjected to microhardness measurement along each scribed line. A Buehler Micromet Micro Hardness Tester with a diamond indenter and a 300 gram load was used to take the measurements. Penetrations

were made at 0.2 mm intervals along the linear traverses, but the intervals were reduced to 0.1 mm in the vicinity of the fusion line.

C. MICROSTRUCTURAL CHARACTERIZATION

After completion of the microhardness measurements, the samples were re-polished, re-etched with Nital for 45 seconds, and examined with a Zeiss ICM 405 microscope. A series of photographs was taken along the HAZ microhardness traverses to represent the weld metal, coarse HAZ, fine HAZ, and base metal regions. Montages comprised of several optical micrographs were prepared of the single-pass HAZ regions to illustrate these locations. Photographs were also taken throughout the last weld pass region of the weld metal and a region of base metal which was unaffected by the welding process. These micrographs were taken at 500x and enlarged to 750x. The grain size in the coarse HAZ region of the last pass was measured for the GMAW and SAW samples using the intercept method.

Scanning electron micrographs were taken at the minimum, average, and maximum hardness locations within the last pass of the weld metal at approximately 2,000x. A Cambridge Stereo S4-10 scanning electron microscope operated at 40 kV was used.

In preparation for transmission electron microscopy, each HAZ sample was wafered along a plane parallel to the plane of the weld fusion line using a low-speed diamond wafering wheel. The weld metal samples were wafered perpendicular to the plane of the fusion line. Figure 4 shows the orientation of these samples and the cutting locations. Wafer thicknesses ranged from 0.35 mm to 0.50 mm. Slices

were numbered commencing with zero, nearest to the weld metal, and increased outward toward the base metal. Each wafer was glued to a flat metal block, sanded and polished to 0.15 mm thickness using standard metallographic techniques. The wafers were etched for 45 seconds in a two-percent Nital solution and optical examination repeated to map the variations of microstructure within each specimen. The wafers were then punched at desired locations to make 3 mm diameter discs. The discs were hand-sanded to a thickness of 0.07 mm using 600 grit paper. These discs were electropolished using a ten-percent perchloric acid-90-percent glacial acetic acid electrolyte solution. Polishing was performed at 40 to 50 volts, 180 to 200 milliamps, and 13° C using a Tenupol twin jet thinning apparatus. The foils were examined with a Jeol 120-CX transmission electron microscope operated at 120 kV.

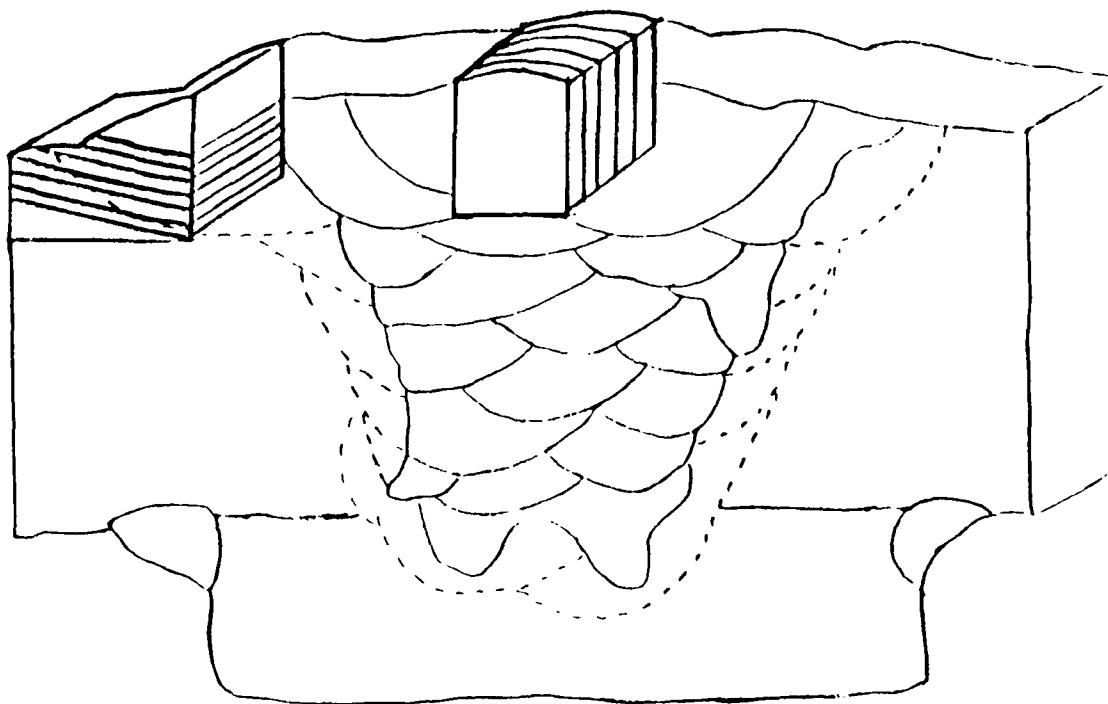


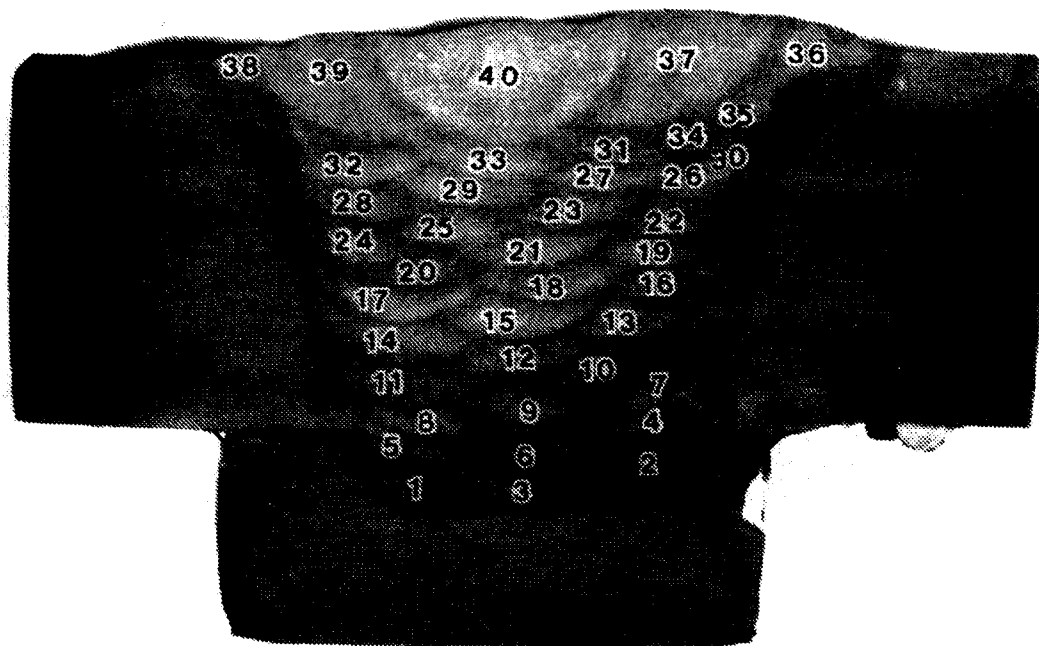
Figure 4. Schematic Showing Orientation of TEM Slices Taken from the Weld Metal and Heat-Affected Zone of the GMAW Weldment

IV. RESULTS

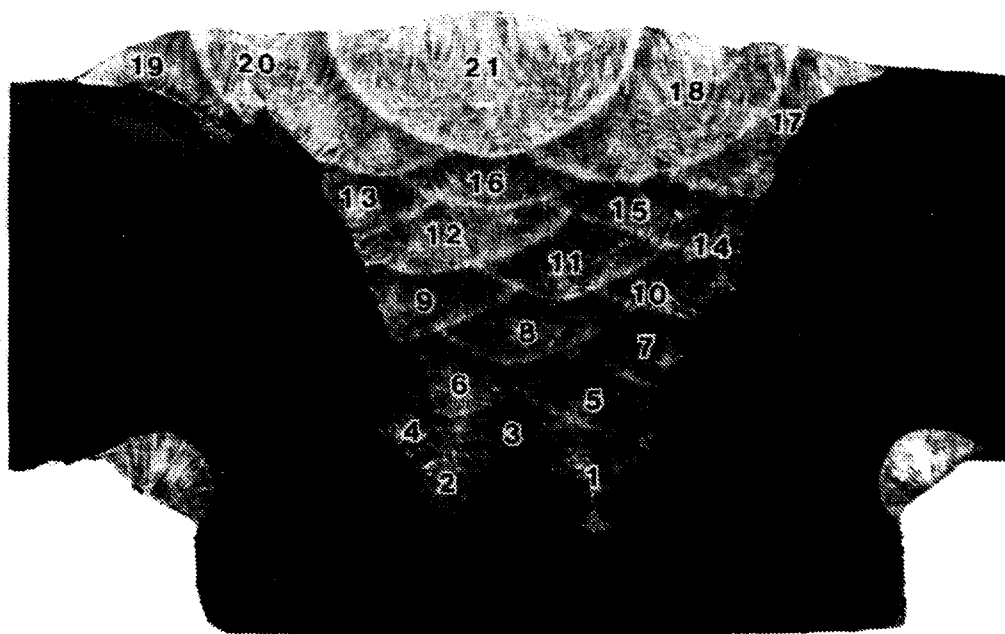
A. MACROSTRUCTURE

Figure 5 (a) and (b) show the etched weldments of the SAW and GMAW processes, respectively. The pass sequence is numbered from one from the first pass to 40 for the last pass in the SAW weldment or 21 for the last pass in the GMAW weldment. The SAW process resulted in much smaller weld beads than the GMAW process and almost double the number of passes (40 versus 21). This is a result of the attempt to keep the weldments as similar as possible. The cooling rates of the two processes were very similar. The last pass was about the same size and located in the center of the weldment for both processes. The papillae are more pronounced and deeper in the GMAW weldment.

Figures 6 and 7 show the montage of weld pass number 36 for the SAW weldment and weld pass number 19 for the GMAW weldment, respectively. These passes were selected for comparison because they are both crown passes which have received little or no thermal cycling. The regions selected within these passes had received no thermal cycling. The weld metal (region A) exhibits a columnar grain structure when Nital was used for etching. The relatively large grains of the coarse HAZ (region B) are clearly visible. The size of these grains appears similar in both processes. Measurements of grain size were performed using the intercept method and optical micrographs



(a)



(b)

Figure 5. Etched Weldments of (a) SAW and (b) GMAW Processes

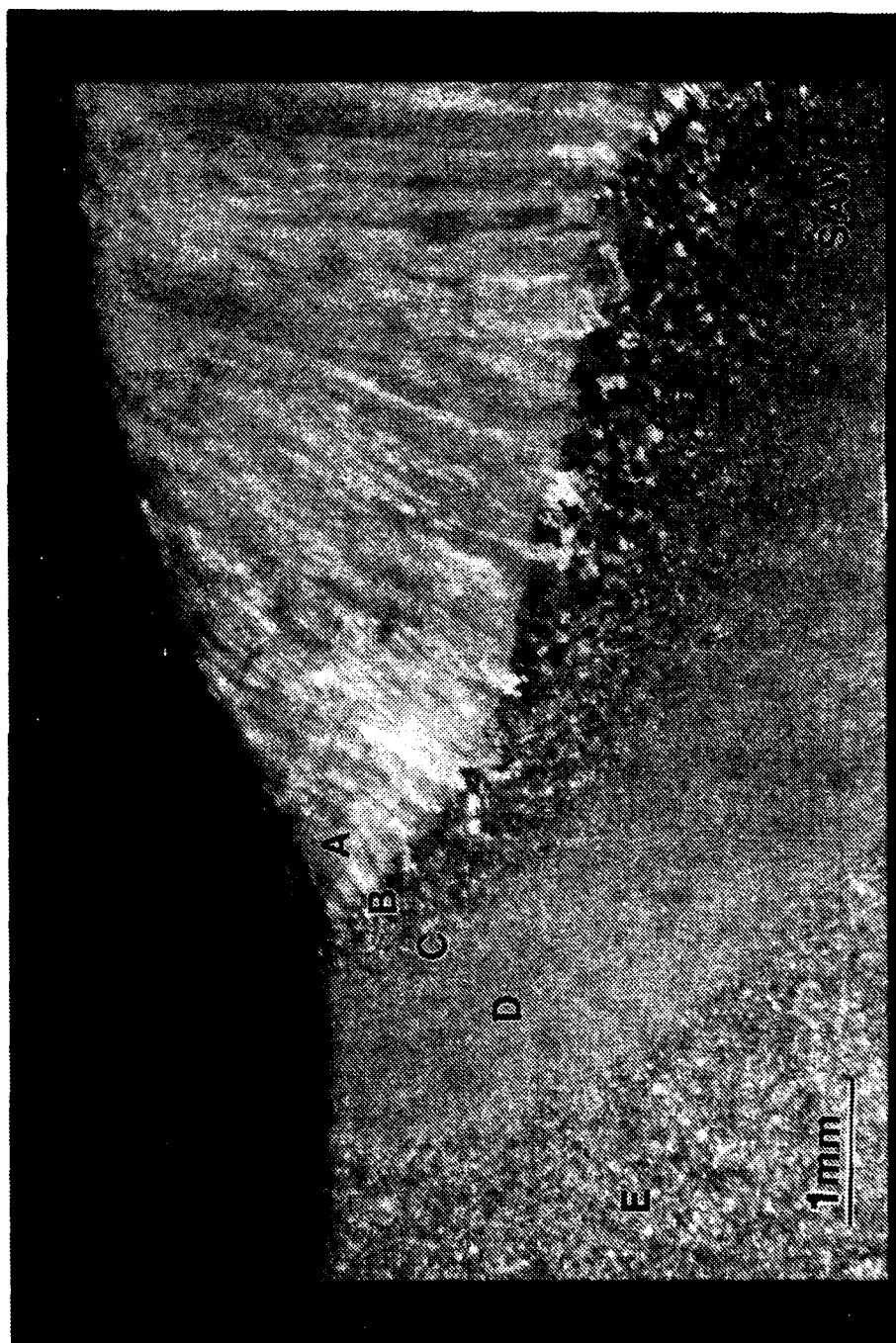


Figure 6. Montage Showing Welding Zones of SAW Weld Pass #36

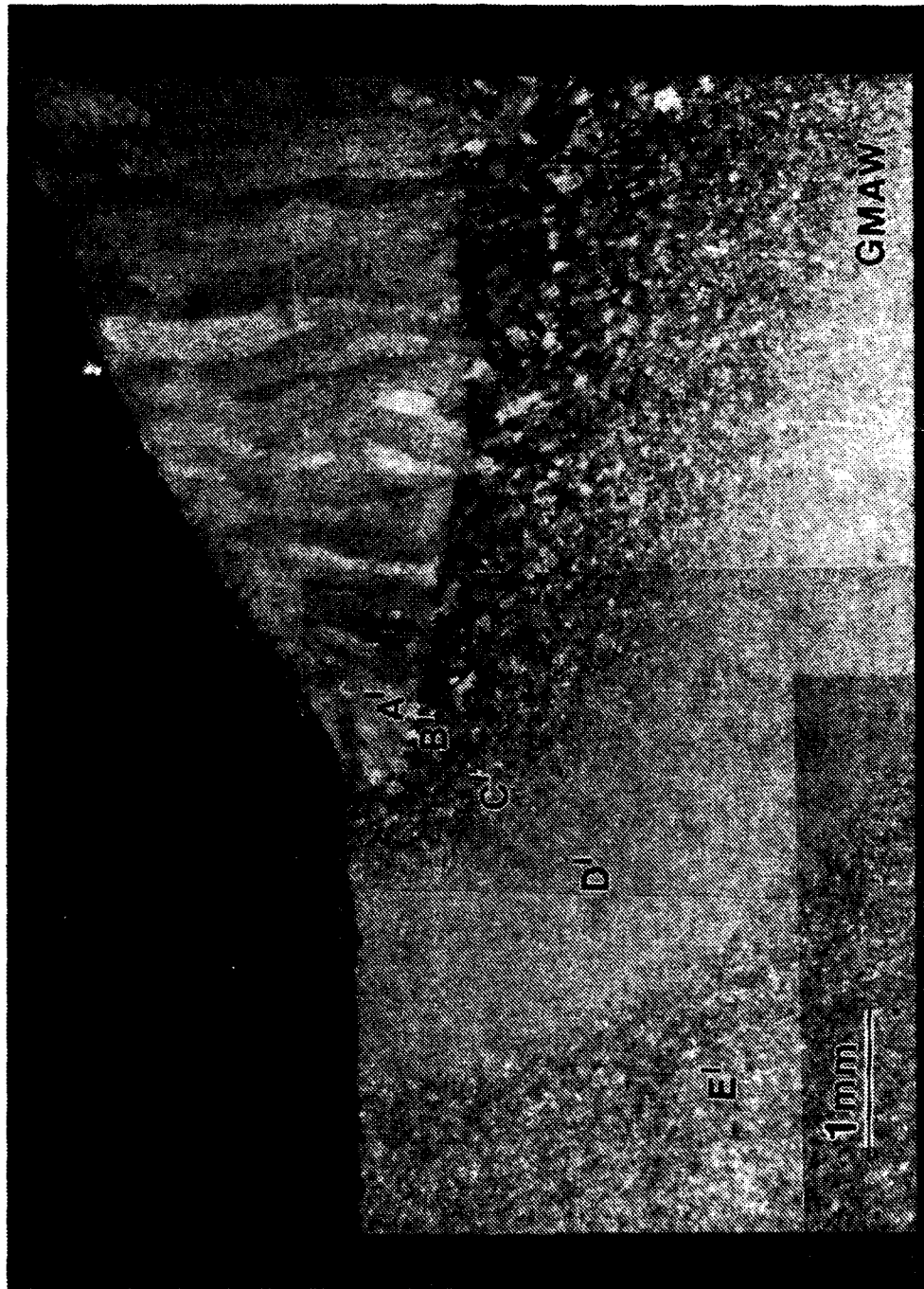


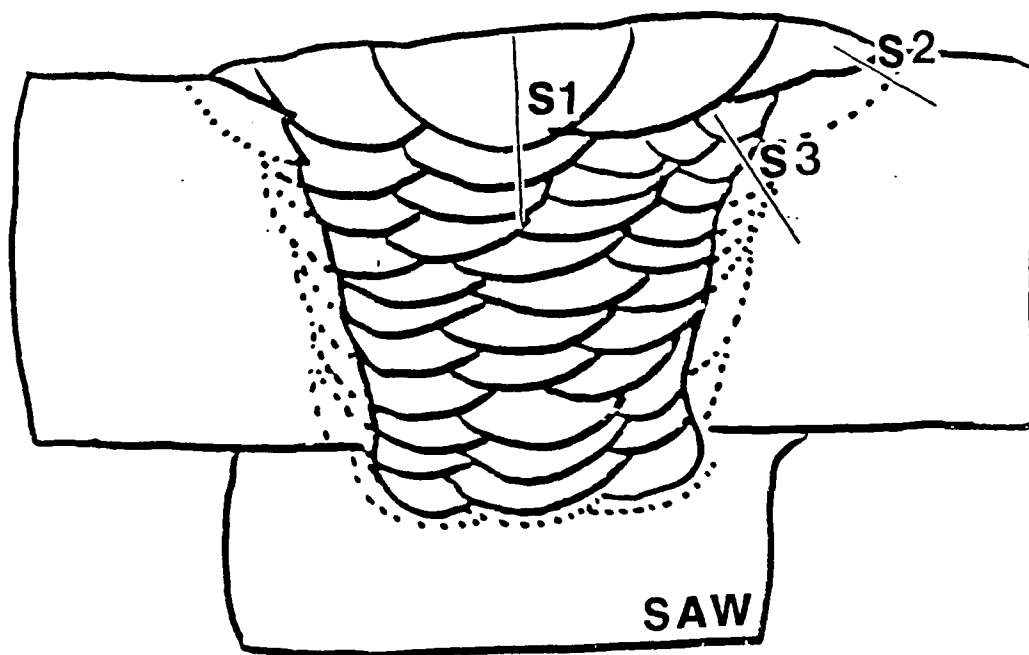
Figure 7. Montage Showing Welding Zones of GMAW Weld Pass #19

at 500x of the coarse HAZ close to the fusion line. The average grain size was 26 μm in the SAW sample and 30 μm in the GMAW sample, which confirmed that the two processes had a similar grain size. It is seen that the grains become much finer, moving from the fusion line toward the base metal. The fine HAZ is marked as region D, while the base metal is marked as region E. The HAZ is narrower at the crown of the weldment and widens toward the root. It appears that the HAZ thickness is greater in the GMAW process.

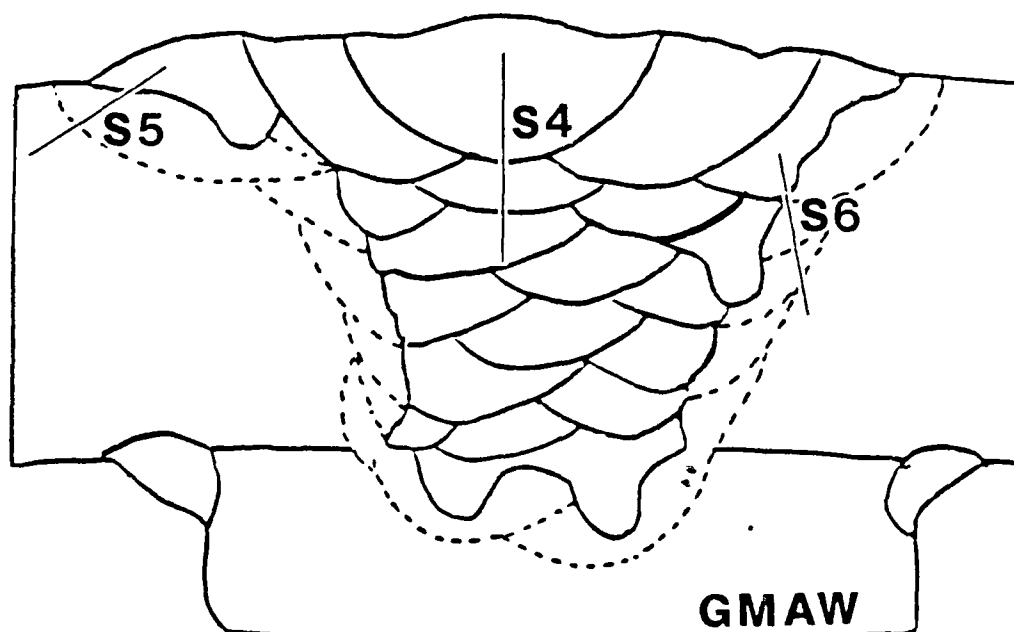
B. MICROHARDNESS MEASUREMENTS

Figure 8 is a schematic representation of the weldments produced by the SAW and GMAW processes to indicate the location of the microhardness traverses. Scribes S1 and S4 are through the center region of the two welds; scribes S2 and S5 are across single-weld passes of no or little thermal cycling (pass number 36 for SAW and pass number 19 for GMAW), and scribes S3 and S6 are across HAZ regions which have experienced considerable thermal cycling. Figures 9, 10, and 11 show the resulting Vicker's microhardness profiles for the scribes through the weld center, across the HAZ of the single pass, and across the thermally cycled HAZ region, respectively.

The profiles through the weld metal (Figure 9) show a major difference between the two processes in that the GMAW weld metal is substantially harder. The last pass of each sample extends about seven millimeters from the crown of the weld to the root of the last pass (indicated by "1" on the profiles). The average hardness of the last



(a)



(b)

Figure 8. Schematic Representation of (a) SAW and (b) GMAW Weldments Showing Locations of Microhardness Traverses

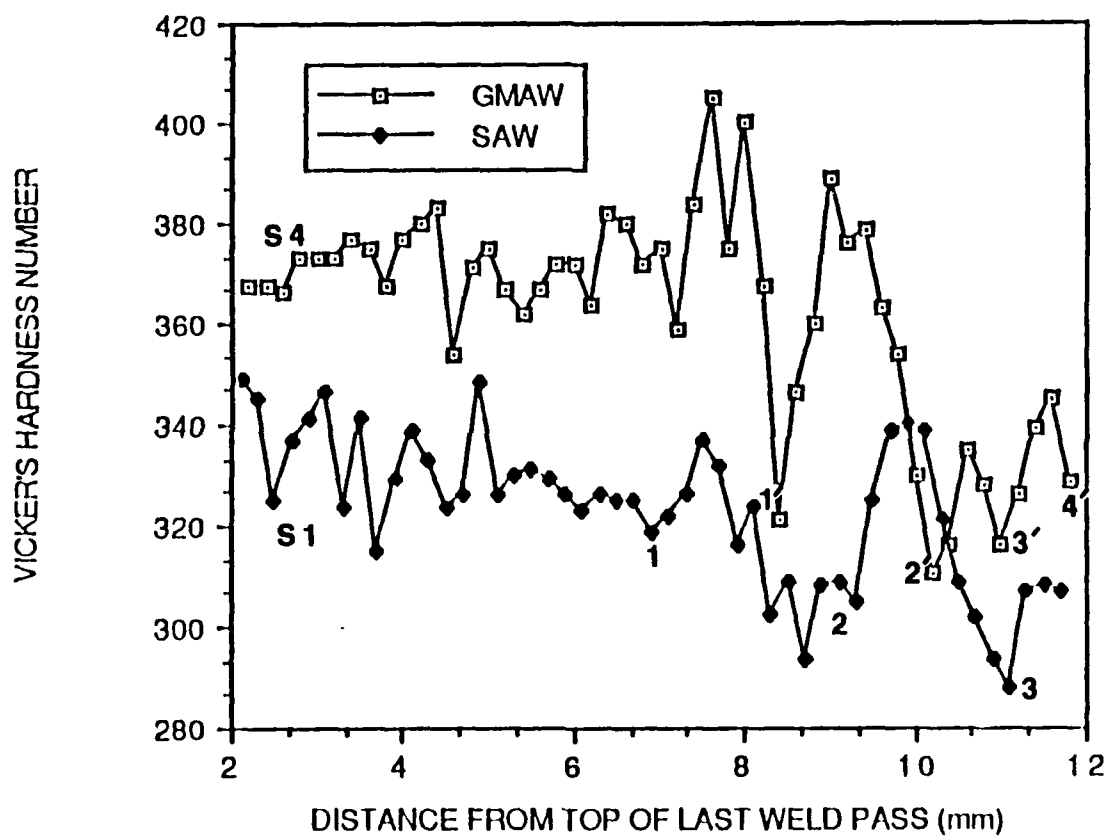


Figure 9. Microhardness Profiles Across the Center of the Weld Metal

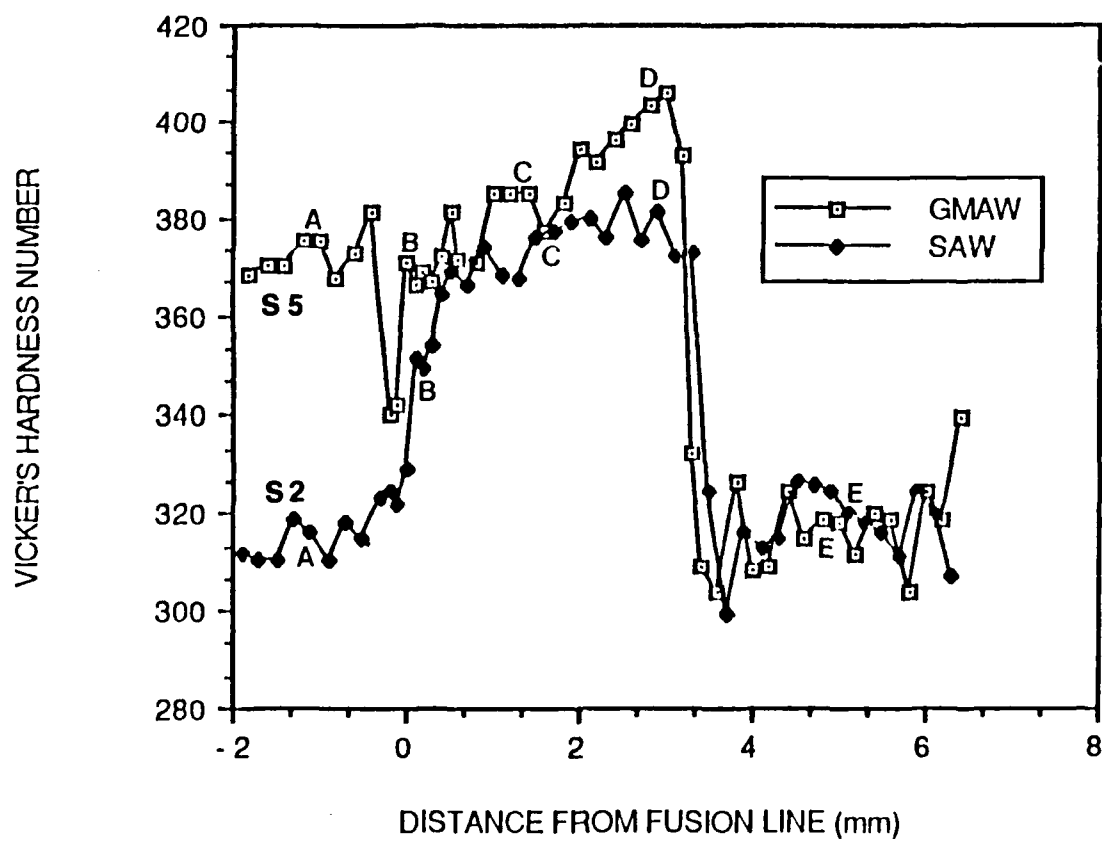


Figure 10. Microhardness Profiles Across the HAZ of a Single-Weld Pass

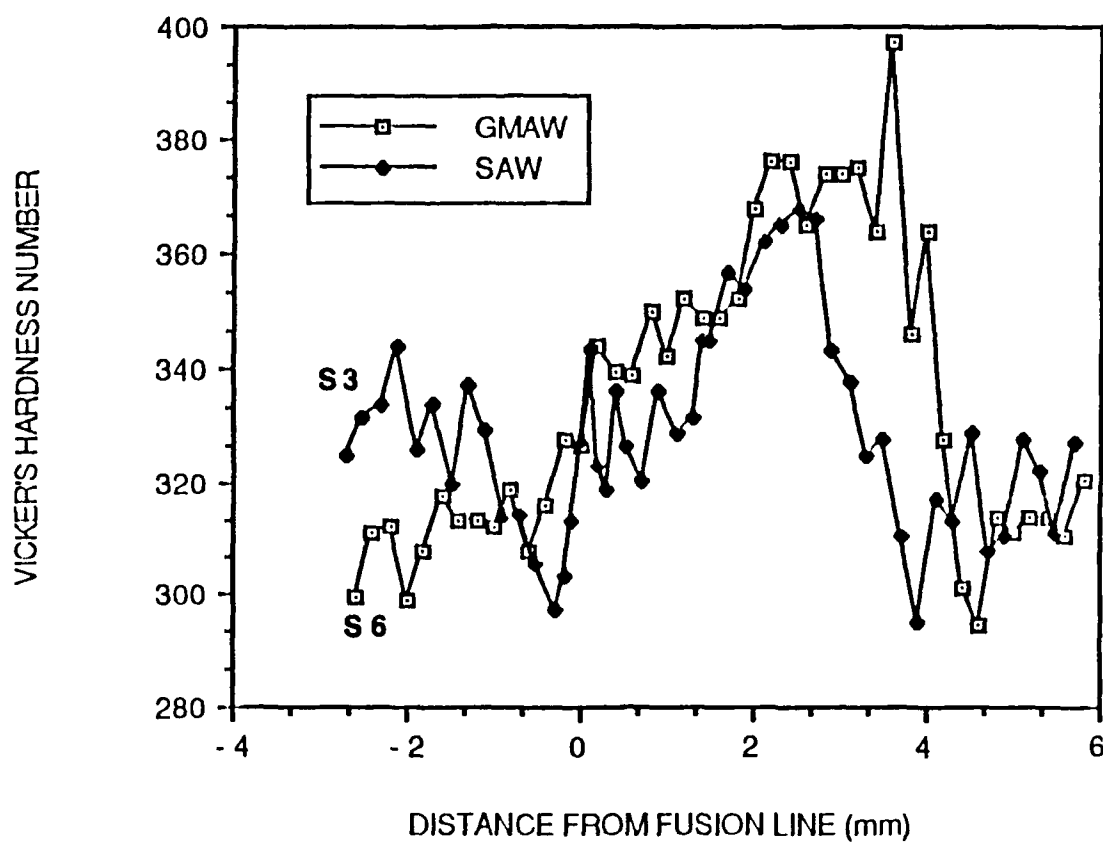


Figure 11. Microhardness Profiles Across the HAZ Affected by Several Thermal Cycles

pass is 371 VHN for the GMAW sample and 333 VHN for the SAW sample. The hardness profiles decrease to minimum points at locations numbered 1, 2, 3, and 4, which correlate with the intersection of two heat zones. The average hardness is reduced for each previous weld pass, as seen in Figure 9.

The microhardness profiles across the HAZ in Figure 10 indicate that both processes follow the same hardness trend in the similar single-pass region. The hardness drops at the fusion line, then sharply increases through the HAZ, displaying two distinct levels. The first plateau identifies the coarse HAZ while the higher second plateau identifies the fine HAZ. The hardness reaches a maximum in the fine HAZ, sharply decreases at the end of the visible HAZ, and then reaches a steady value of approximately 317 VHN in the base metal. The GMAW sample exhibits a much larger decrease in hardness at the fusion line than the SAW sample. The GMAW sample is slightly harder throughout the HAZ, reaching a maximum hardness of 406 VHN compared to a maximum of 385 VHN for the SAW process. It is coincidental that the width of the HAZ is approximately 3.4 mm for both processes at the location of S2 and S4. In general, however, the width of the HAZ varies significantly with the location in the HAZ and the angle of the scribe. The slope of the hardness profile, when passing from the fine HAZ into the base metal, is about the same. A pronounced difference was, however, observed in the hardness of the weld metal.

With repeated thermal cycling, the profiles across the HAZ (Figure 11) exhibited a similar microhardness trend as the profiles

with no thermal cycling (Figure 10). The hardness in both processes decreases at the fusion line, increases at about the same slope throughout the HAZ, and decreases with the same slope to a steady value of about 316 VHN in the base metal. The maximum hardness in the fine HAZ was 397 VHN for the GMAW process and 367 VHN for the SAW process.

Rockwell C hardness measurements taken in the base metal indicated an average hardness of 42 Rc.

Five distinct regions characterized by the microhardness trends of Figures 9 and 10 were selected for microstructural investigation. These regions are:

- a. base metal (region E),
- b. weld metal of last pass (pass numbers 40 and 21),
- c. weld metal close to coarse HAZ (region A)
- d. coarse HAZ (region B), and
- e. fine HAZ (region D).

The region labeled C on Figures 6 and 7 was an intermediate region of the HAZ. There was not a distinct transition between the coarse HAZ and fine HAZ, so it was difficult to correlate this location between the SAW and GMAW weldments. For this reason, no microstructural analysis was done at this location.

C. MICROSTRUCTURAL CHARACTERIZATION

The selected regions were examined using optical, scanning, and transmission electron microscopy. The microstructure of the base

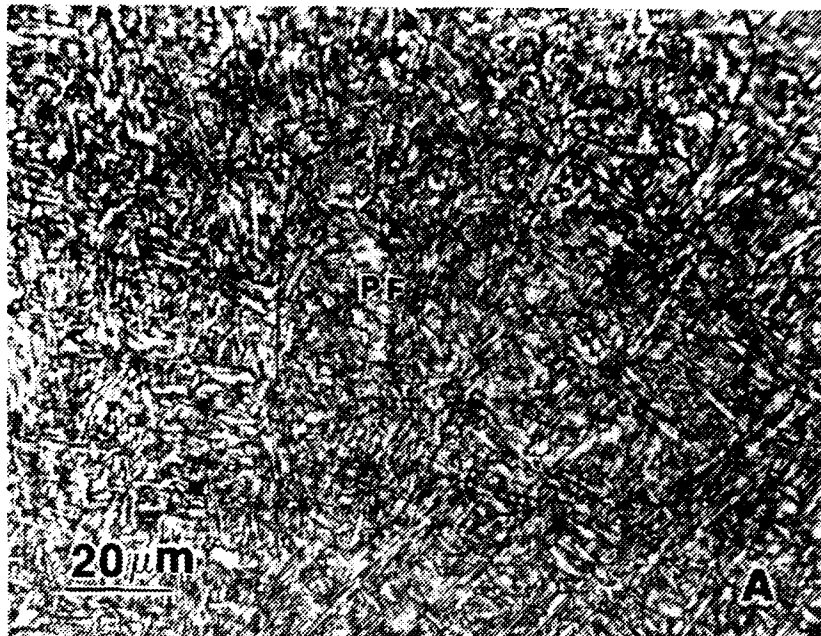
metal, weld metal, and HAZ of the SAW and GMAW processes were characterized and compared.

1. Optical Microscopy

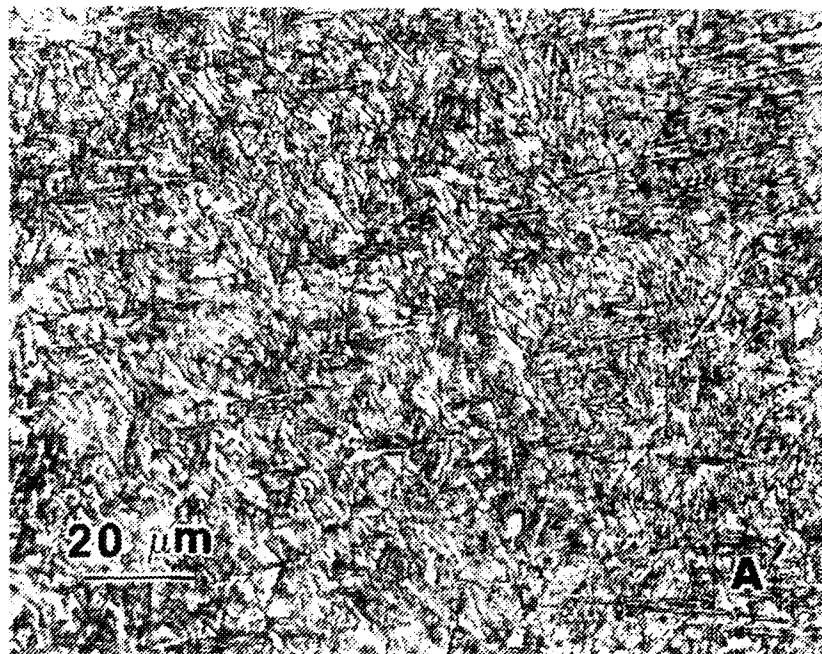
Optical micrographs of the SAW and GMAW weldments across the HAZ of the passes illustrated in Figure 6 and 7 are compared in Figures 12 through 15. The weld metal of both processes (Figure 12) appeared to have a fine martensitic-bainitic structure. Some polygonal ferrite can be seen and is indicated in the GMAW micrograph. The coarse HAZ of both weldments (Figure 13) consisted predominantly of a lath martensite structure, although in some areas a bainitic structure was also present. Packets of martensite containing parallel laths can be readily resolved within the coarse prior austenite grain boundaries. Some plate martensite was occasionally found. The fine HAZ in both processes (Figure 14) consisted of a much finer martensitic-bainitic structure, but the prior austenite grain boundaries were not delineated in this zone by the two-percent Nital etching technique used. The microstructure of the base metal (Figure 15) consisted of a tempered martensite-bainite duplex structure.

2. Scanning Electron Microscopy (SEM)

SEM was employed because it was difficult to distinguish between the microstructural differences between the two welding processes under optical examination. SEM was performed in the weld metal to observe any microstructural difference corresponding to the variations in hardness. SEM micrographs taken along traverses S1 and



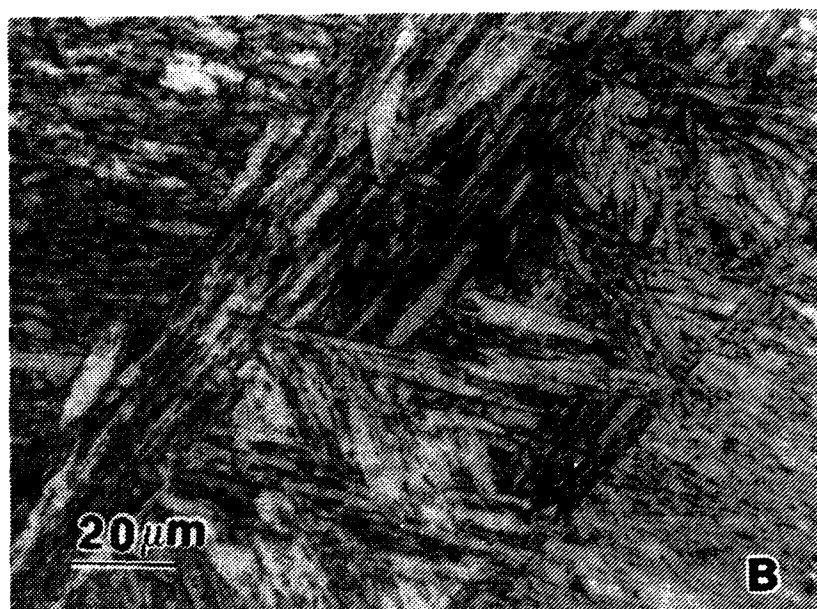
(a)



(b)

PF = polygonal ferrite

Figure 12. **Optical Micrographs of the (a) SAW and (b) GMAW Weld Metal (750x)**



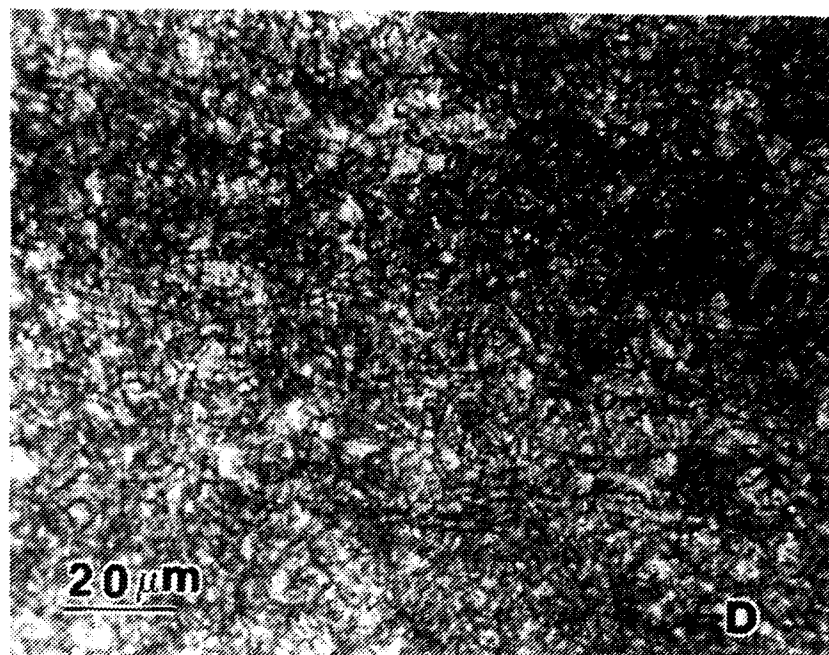
(a)



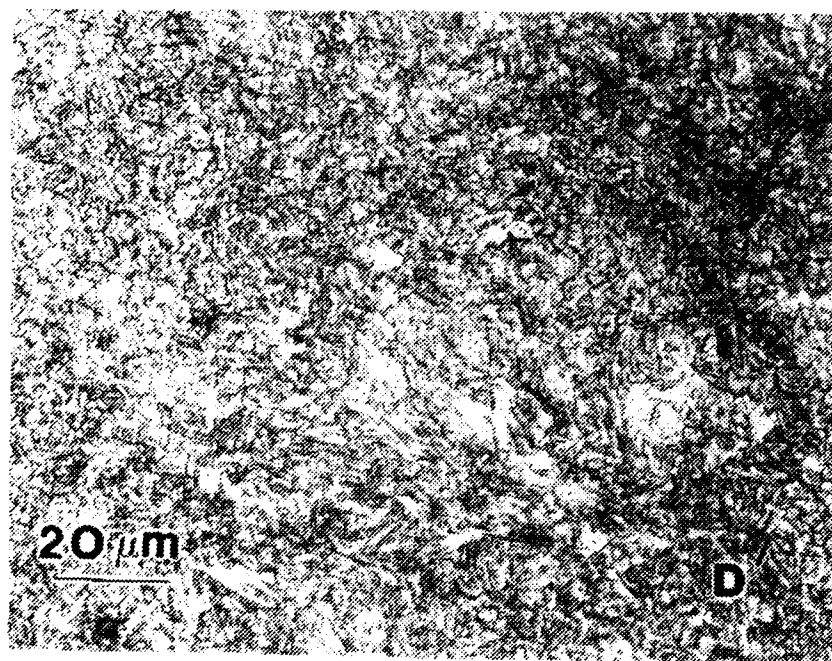
(b)

PM = plate martensite

Figure 13. Optical Micrographs of the (a) SAW and (b) GMAW Coarse HAZ (750x)

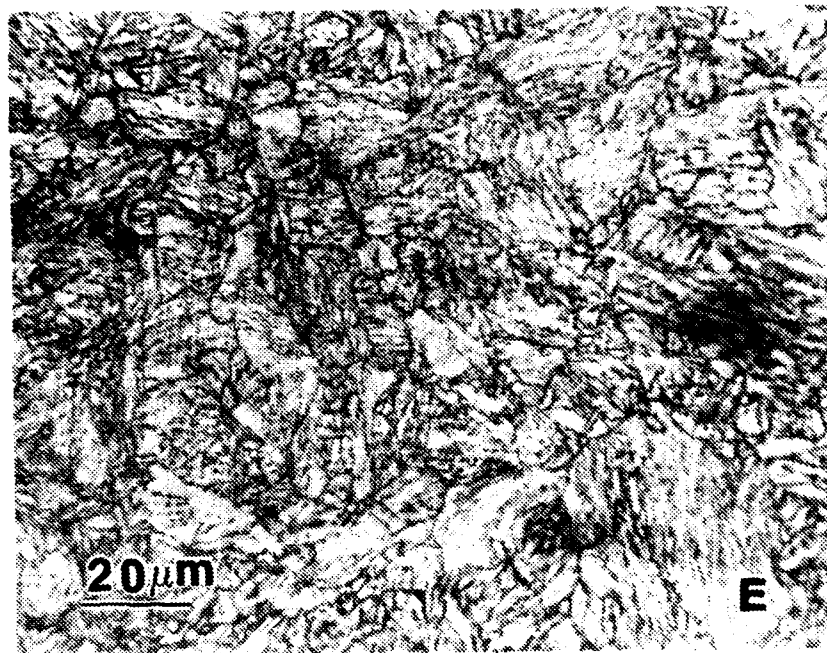


(a)

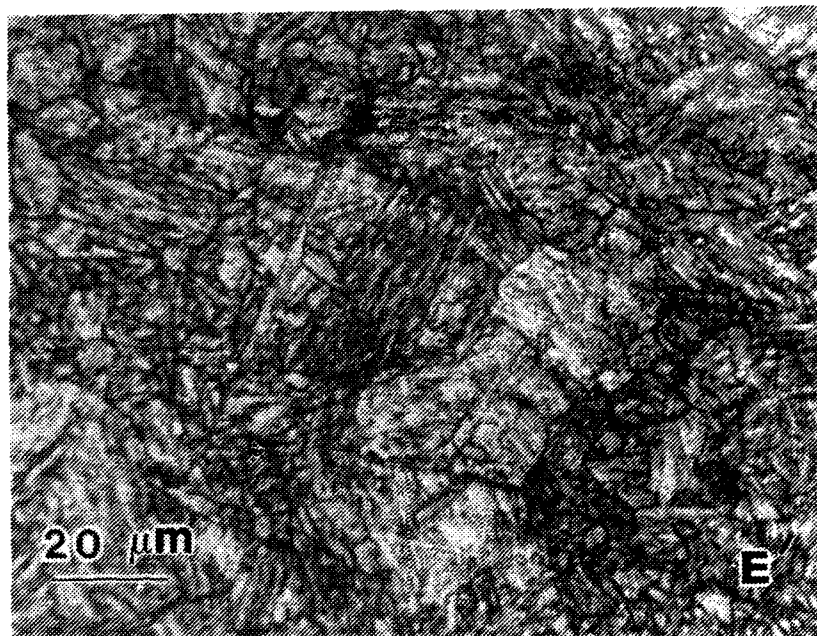


(b)

Figure 14. Optical Micrographs of the (a) SAW and (b) GMAW Fine HAZ (750x)



(a)



(b)

Figure 15. **Optical Micrographs of the (a) SAW and (b) GMAW Base Metal (750x)**

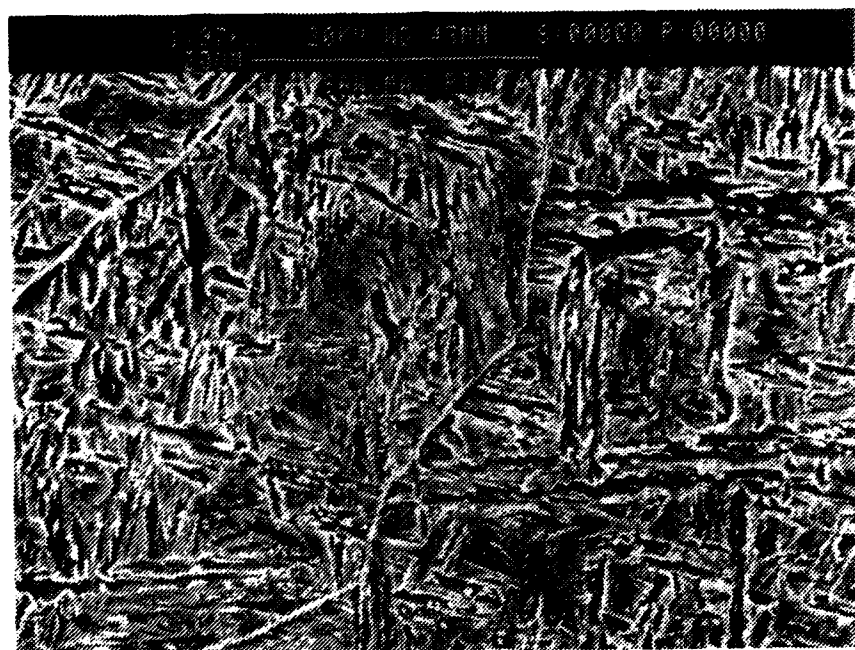
S4 at the maximum, average, and minimum hardness points are shown in Figures 16, 17, and 18, respectively. The hardness values at these locations were 352, 333, and 288 VHN for the SAW process and 405, 373, and 301 for the GMAW process (Figure 9). Both samples showed a similar lath structure, but the GMAW weld metal appeared to have a more defined lath morphology. Even at the SEM resolution level, comparison between the weld metal structures of the two welding processes was found to be difficult. For this reason, SEM was not completed on regions B, C, D, and E.

3. Transmission Electron Microscopy (TEM)

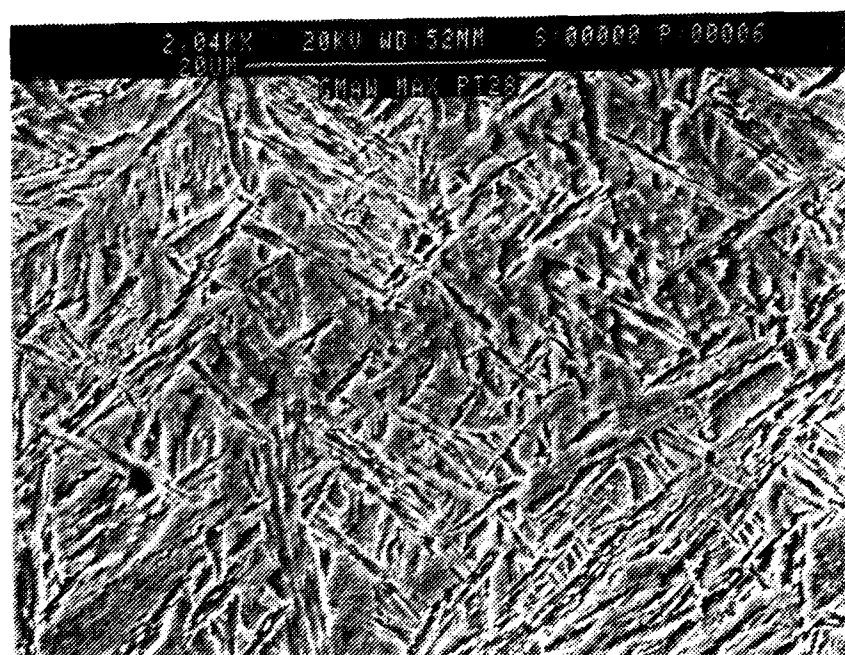
TEM was performed on the same five regions described in the microhardness section and representative microstructures are shown in Figures 19 through 23. In general, both weldments showed the similar microconstituents, but the relative amounts of the microconstituents varied from one weldment to another. Typical microstructures included tempered and autotempered martensite, lath martensite, bainite, retained austenite between the laths, and polygonal ferrite. The microstructure of the GMAW weld metal consisted of more lath martensite and was finer than the SAW weld metal. The microstructure throughout the HAZ of the two welding processes was very similar.

a. Base Metal

Figure 19(a) is a typical micrograph of the base metal region showing the tempered lath martensite structure. Signs of

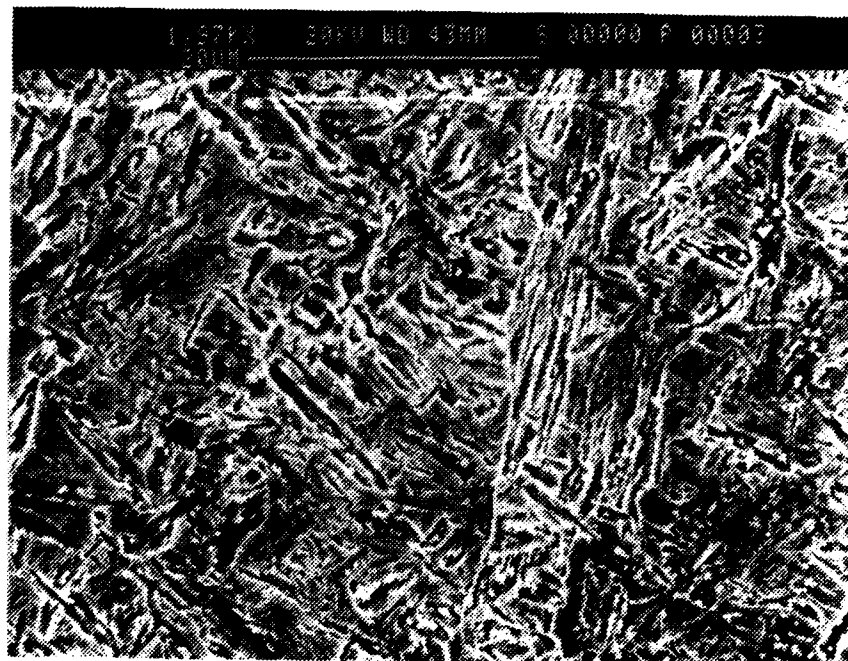


(a)

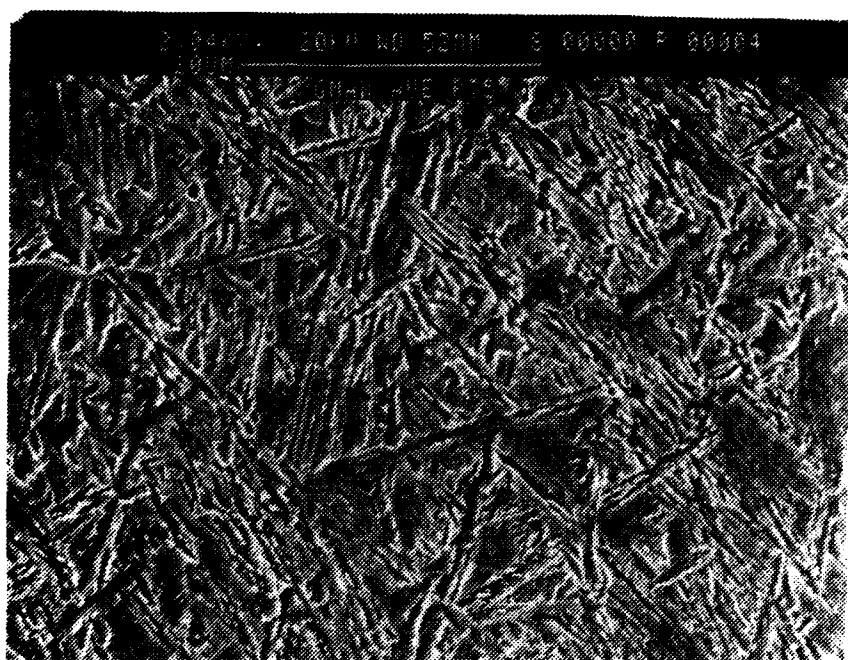


(b)

Figure 16. SEM Micrographs Taken at the Maximum Microhardness Location of the Weld Metal of the Last Pass for (a) SAW and (b) GMAW (approx. 2,000x)

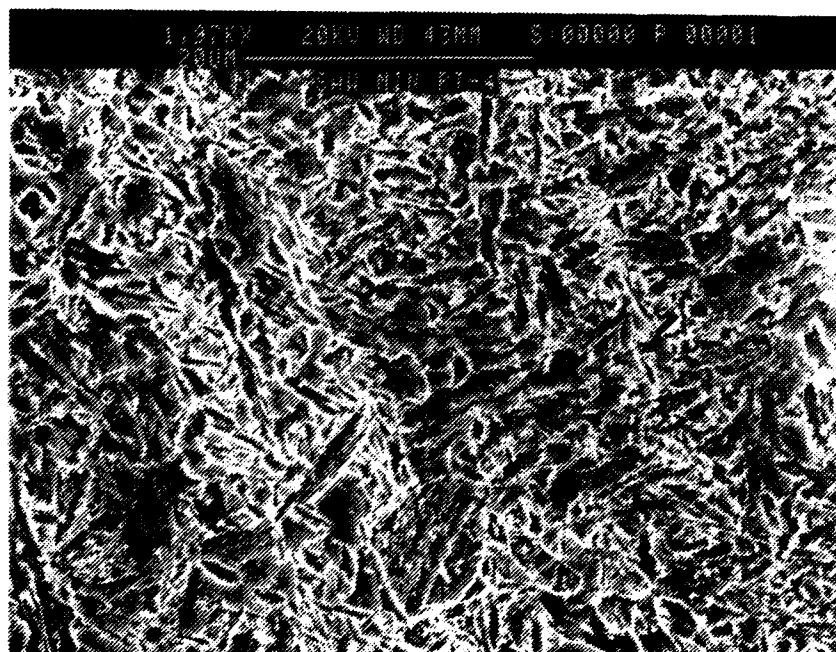


(a)

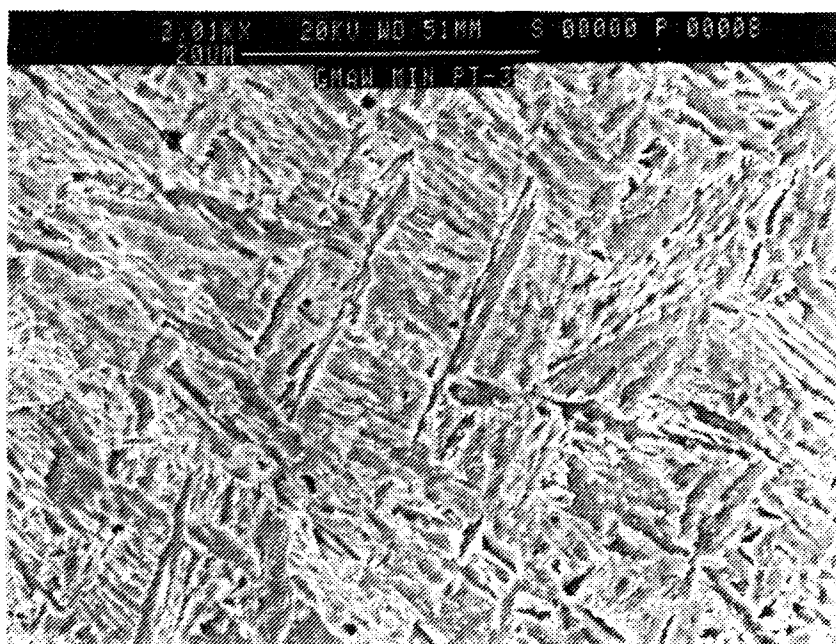


(b)

Figure 17. SEM Micrographs Taken at the Average Microhardness Location of the Weld Metal of the Last Pass for (a) SAW and (b) GMAW (approx. 2,000x)

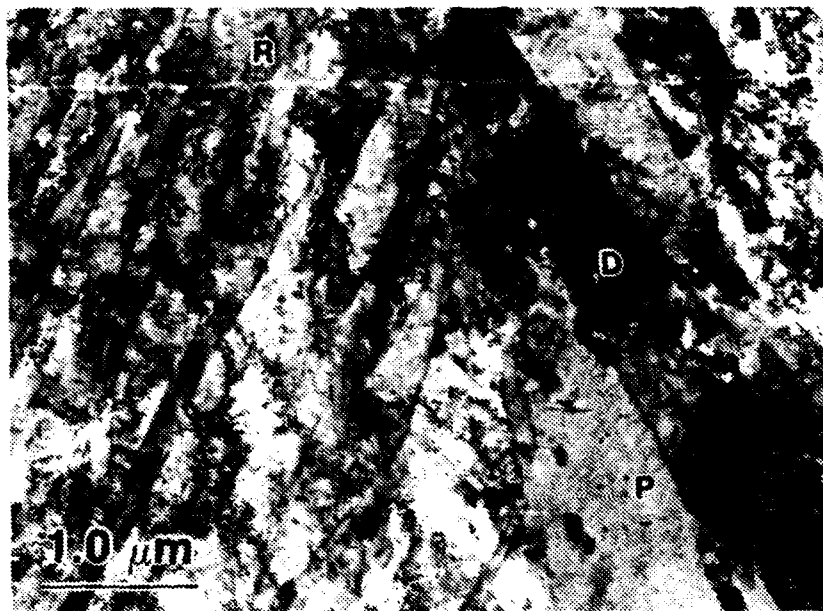


(a)

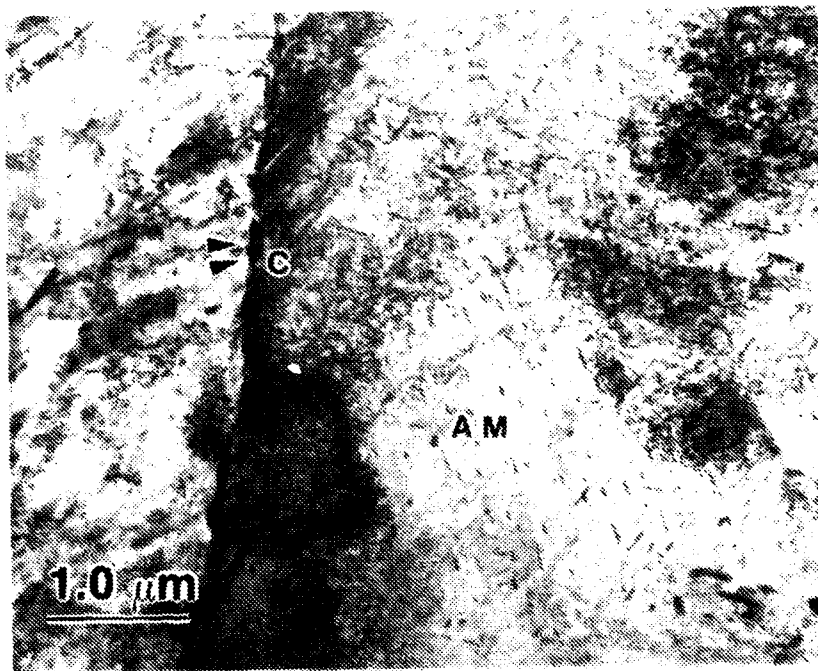


(b)

Figure 18. SEM Micrographs Taken at the Minimum Microhardness Location of the Weld Metal of the Last Pass for (a) SAW and (b) GMAW (approx. 750x)



(a)

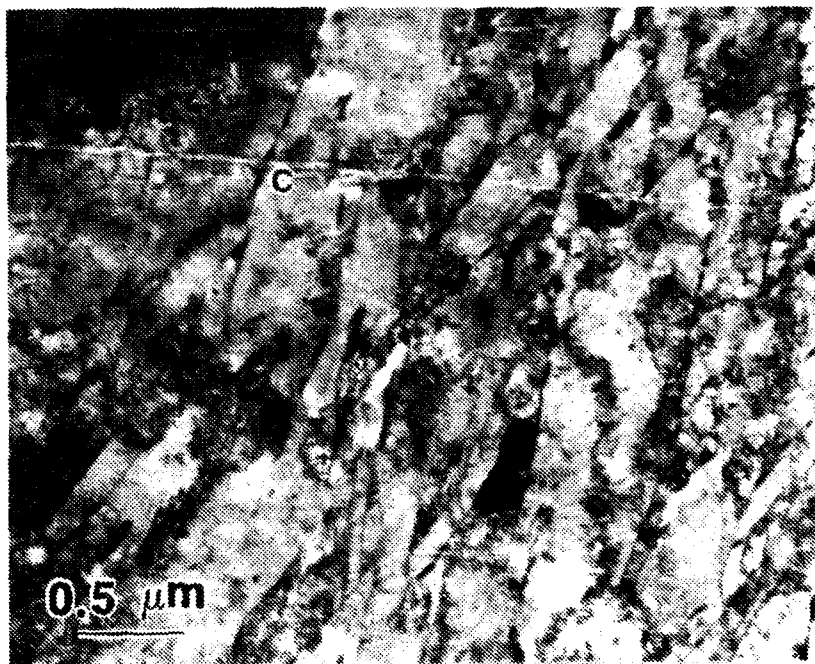


(b)

R = recovery
 P = precipitates
 D = high dislocation density

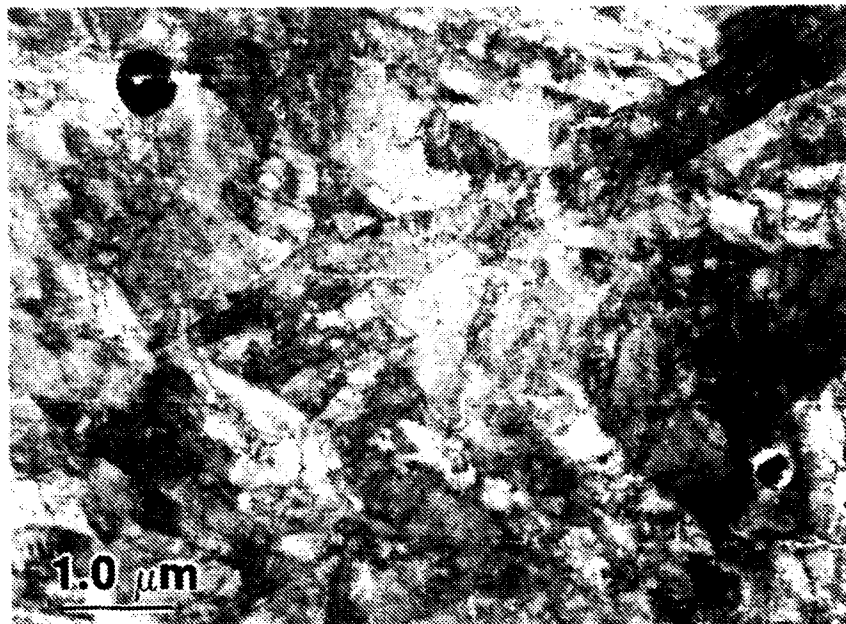
AM = autotempered martensite
 C = cementite

Figure 19. TEM Micrographs in the Base Metal

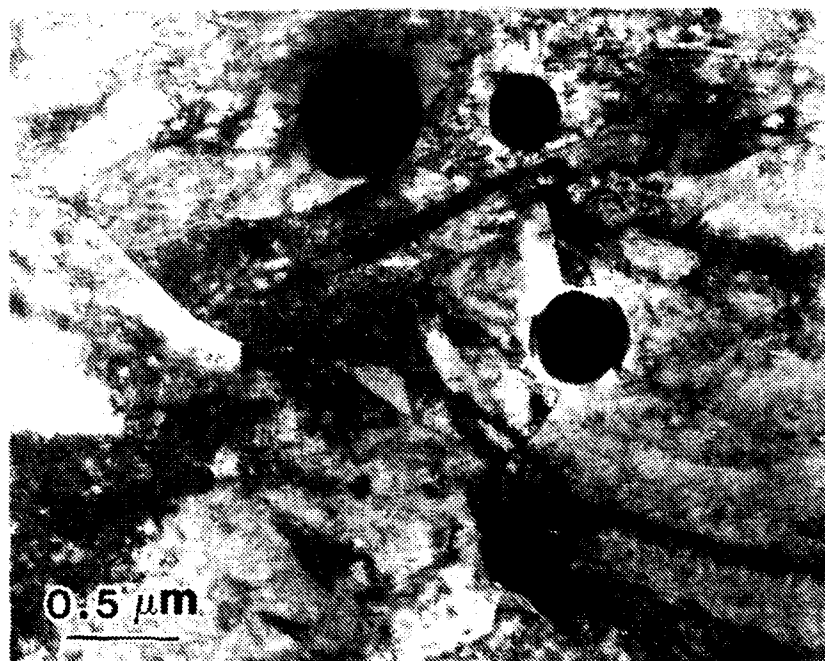


(c)

Figure 19. **TEM Micrographs in the Base Metal** (continued)



(a)



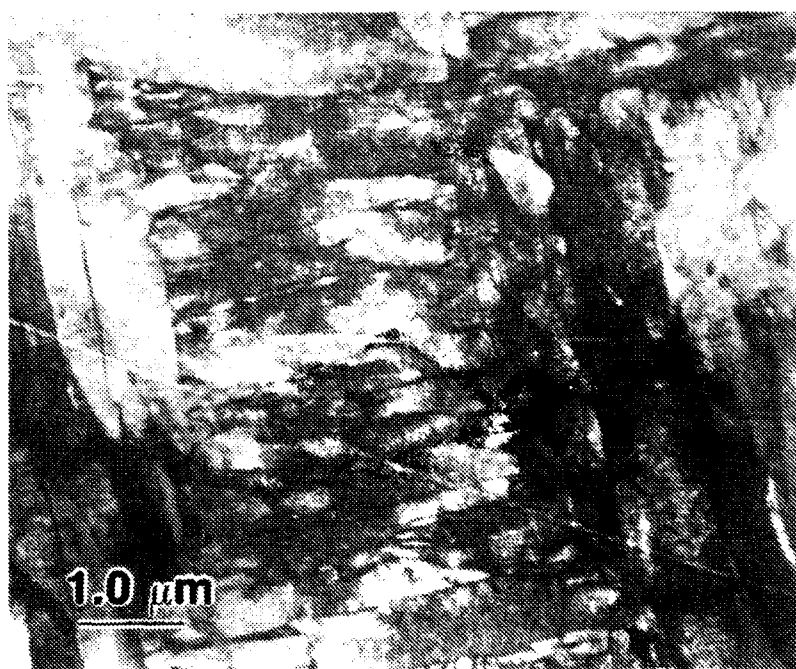
(b)

RA = retained austenite

Figure 20. **TEM Micrographs of the Last Pass Weld Metal**

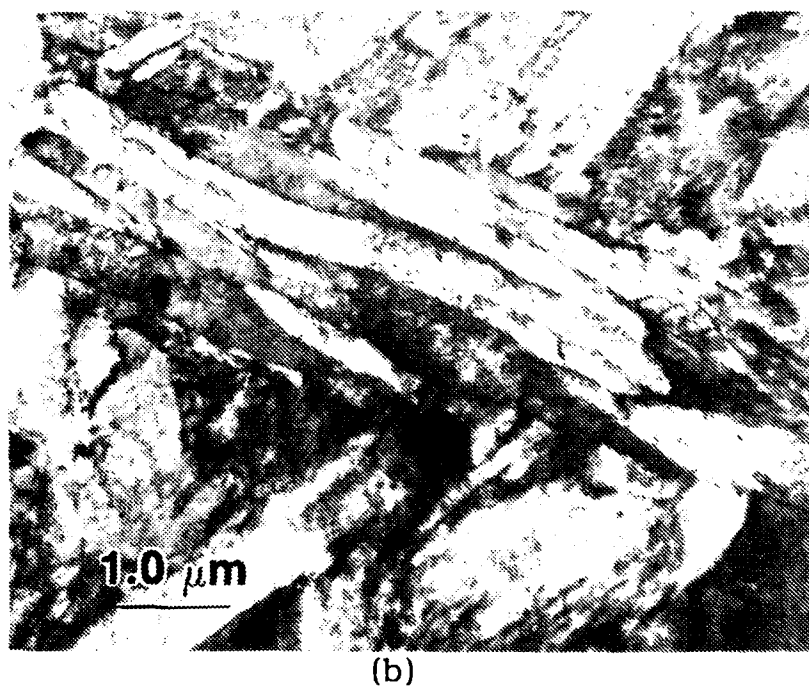
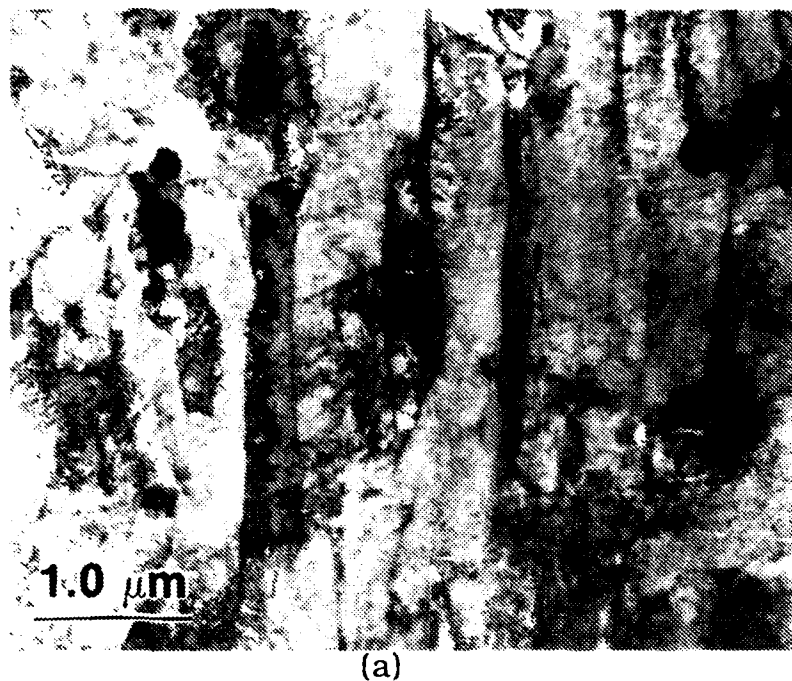


(c)



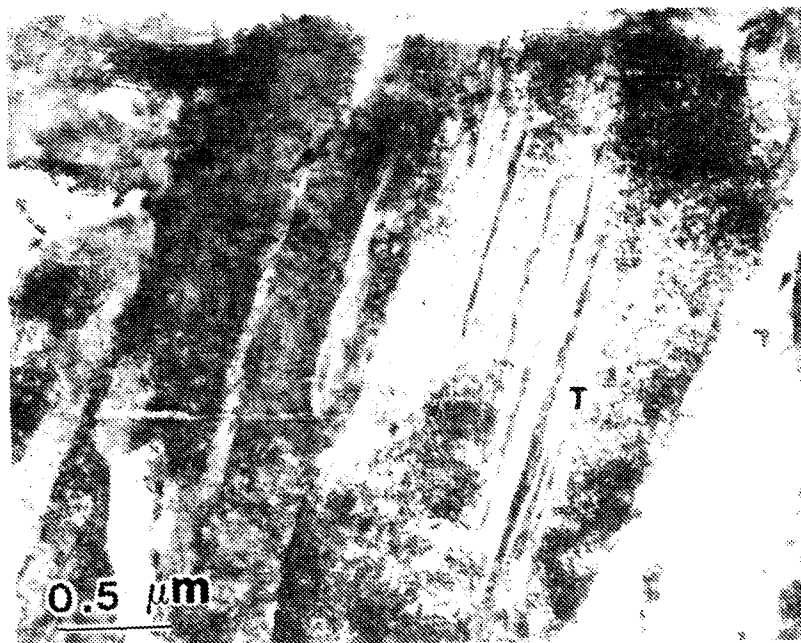
(d)

Figure 20. TEM Micrographs of the Last Pass Weld Metal
(continued)



T = twinned martensite

**Figure 21. TEM Micrographs of Weld Metal Close to Fusion Line
of SAW Pass #36 and GMAW Pass #19**

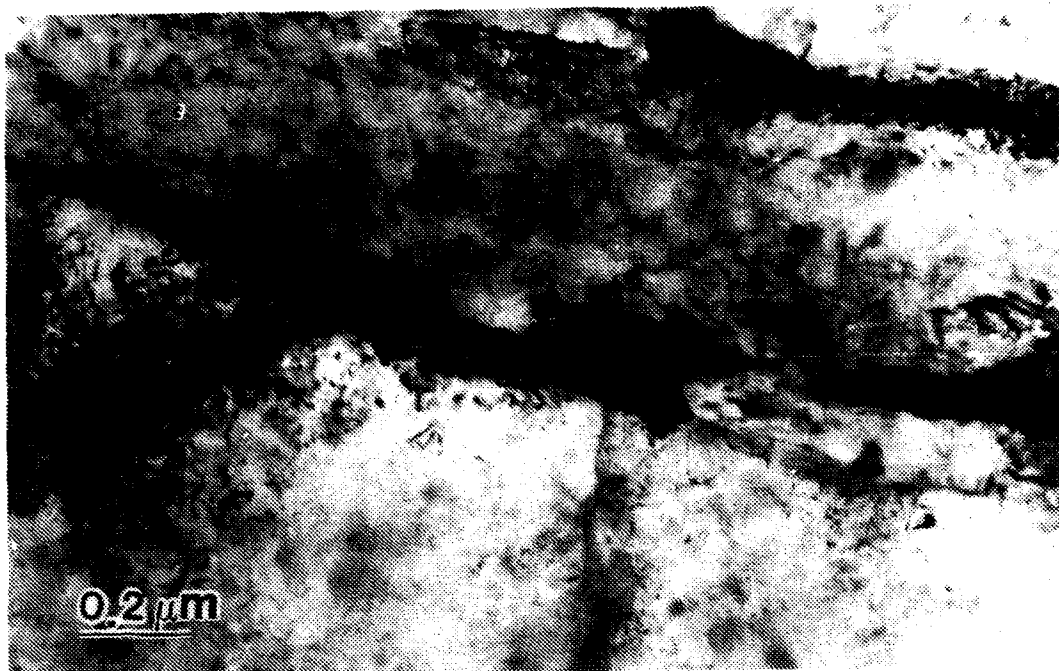


(c)

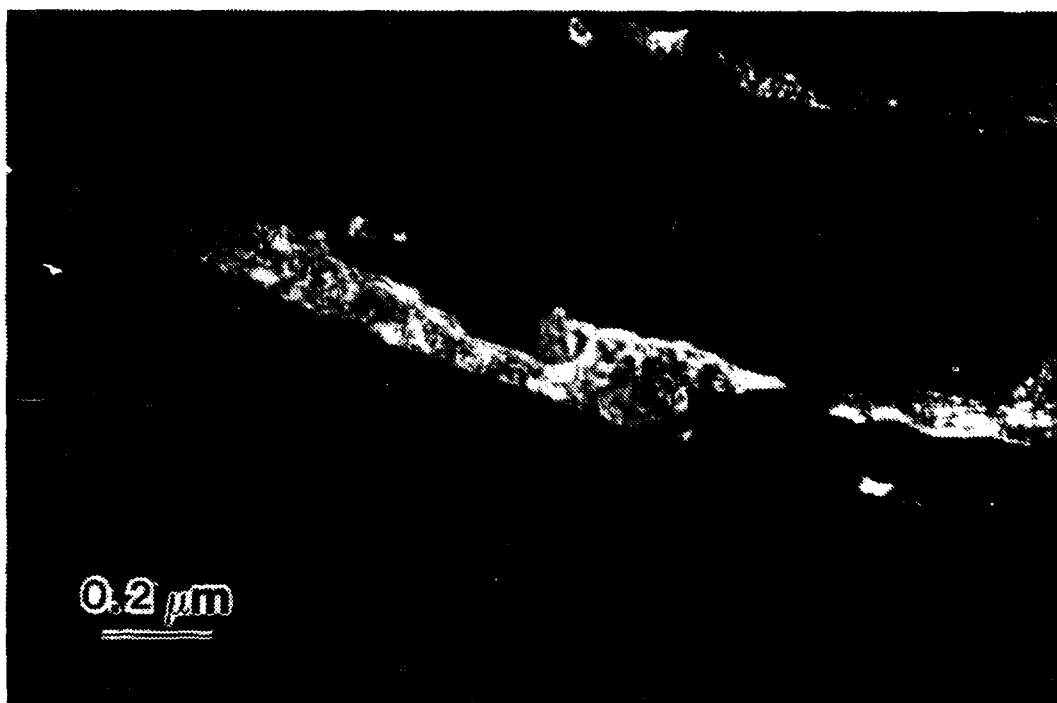


(d)

Figure 21. TEM Micrographs of Weld Metal Close to Fusion Line of SAW Pass #36 and GMAW Pass #19 (continued)

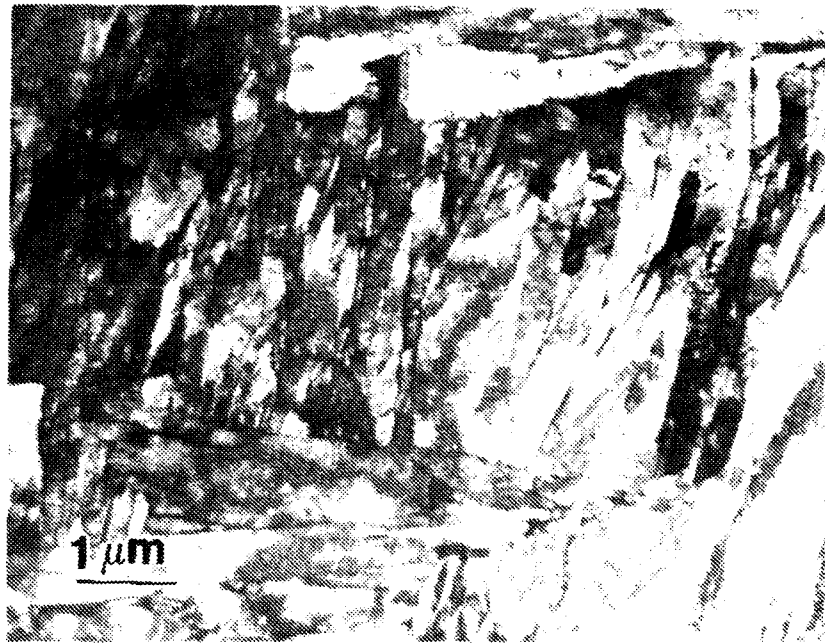


(e)

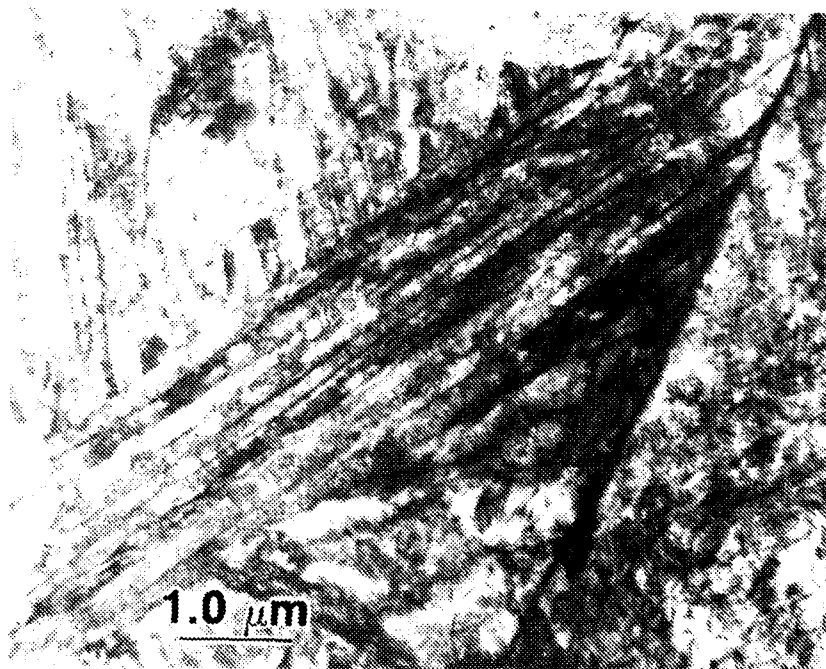


(f)

Figure 21. TEM Micrographs of Weld Metal Close to Fusion Line of SAW Pass #36 and GMAW Pass #19 (continued)

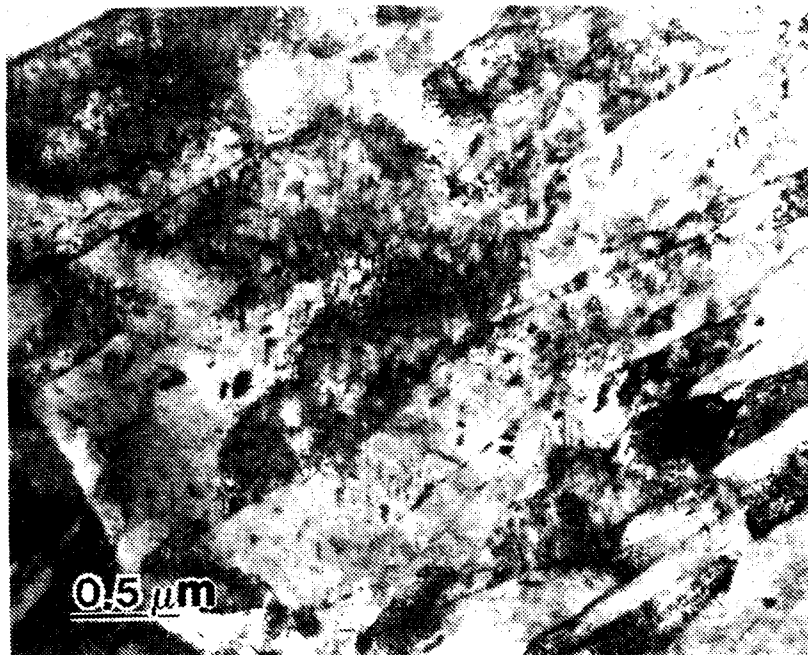


(a)

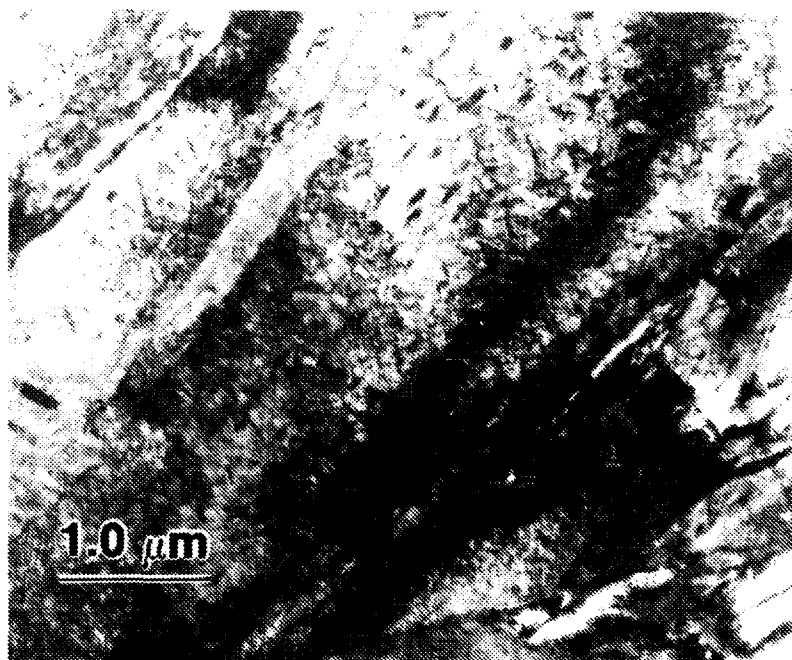


(b)

Figure 22. TEM Micrographs of the Coarse HAZ

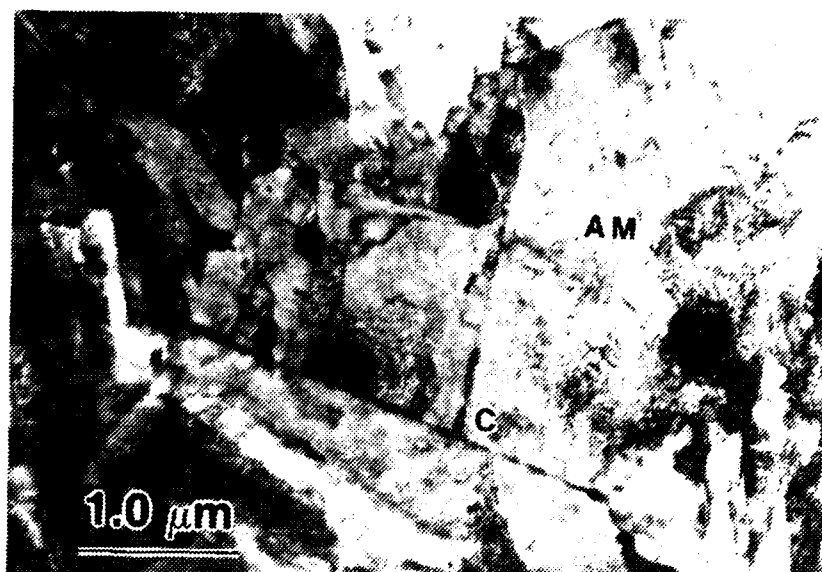


(c)

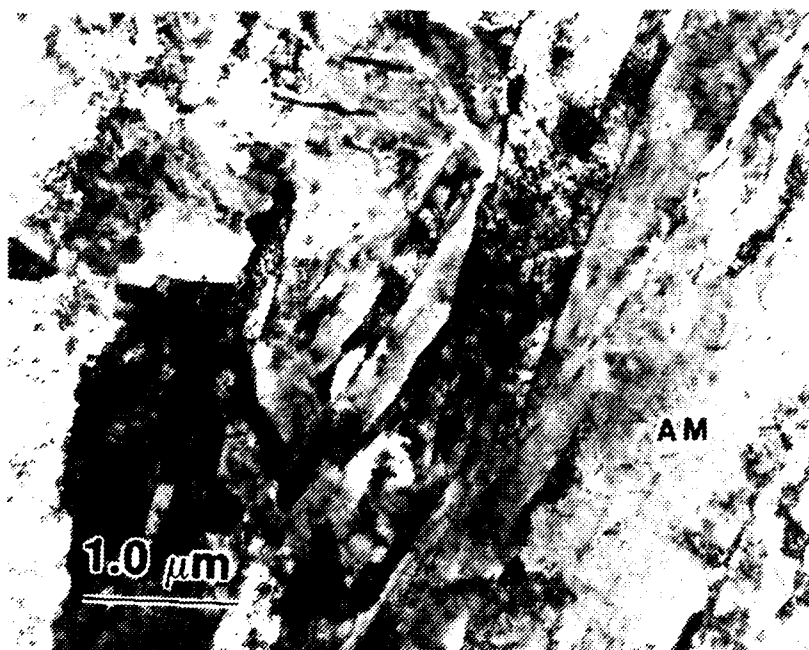


(d)

Figure 22. **TEM Micrographs of the Coarse HAZ** (continued)



(a)

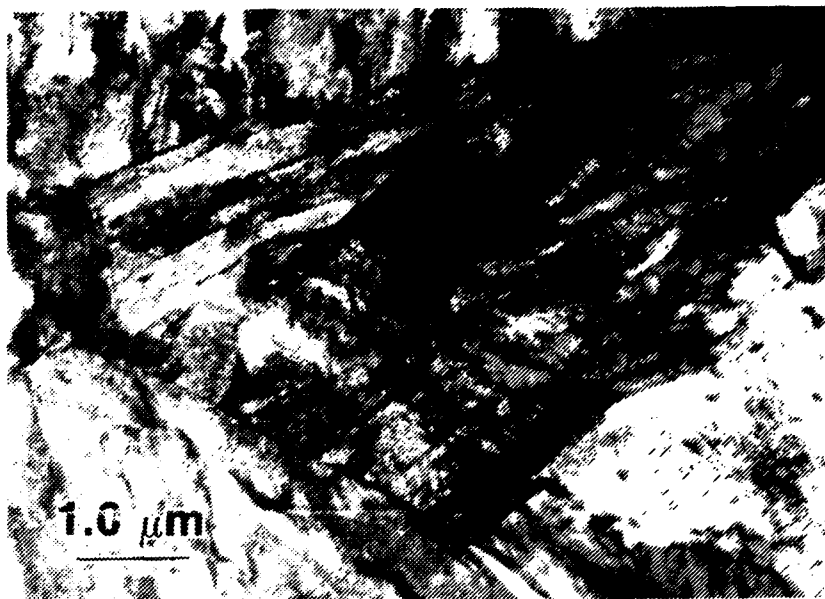


(b)

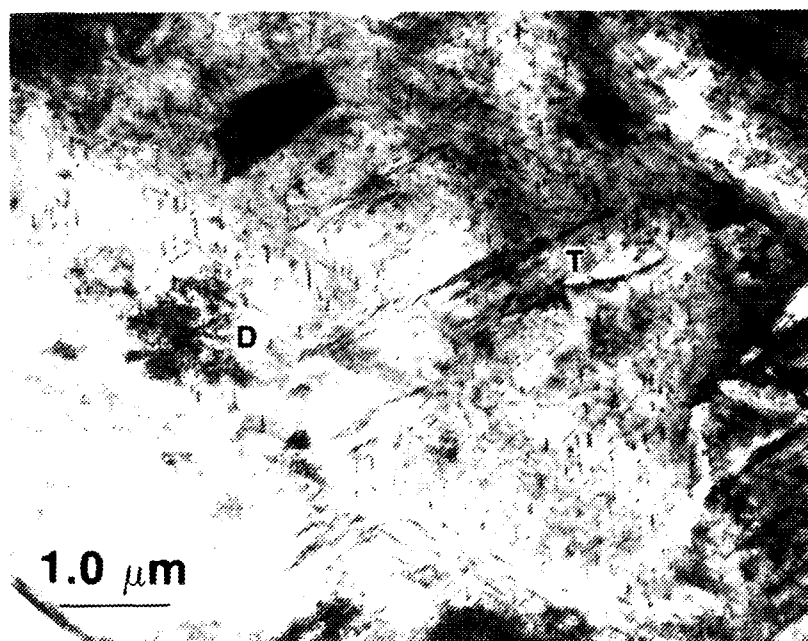
AM = autotempered martensite
T = twinned martensite

C = cementite
D = high dislocation density

Figure 23. TEM Micrographs of the Fine HAZ from SAW and GMAW TEM Slices #3 (a and b), Respectively, from GMAW TEM Slice #4 (c and d), and from SAW TEM Slice #5 and GMAW Slice #7 (e and f), Respectively

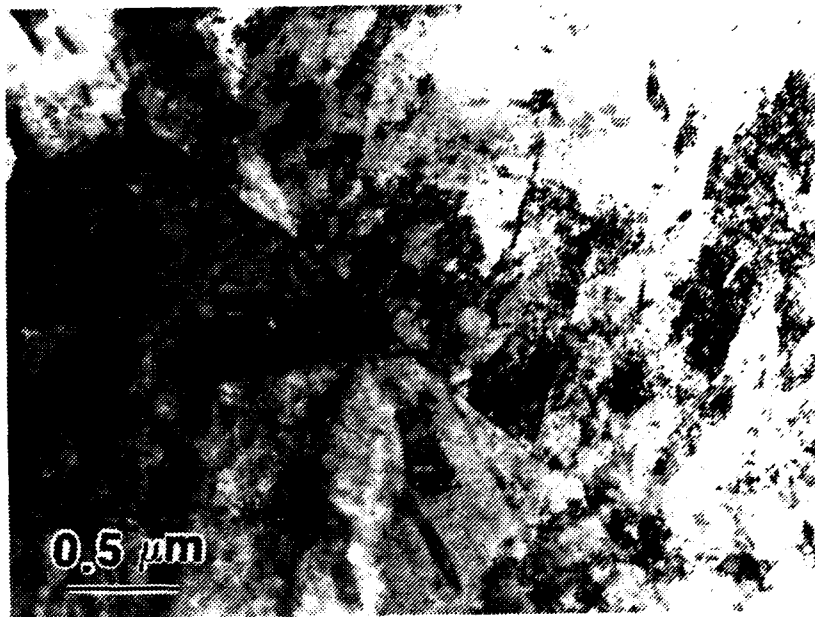


(c)

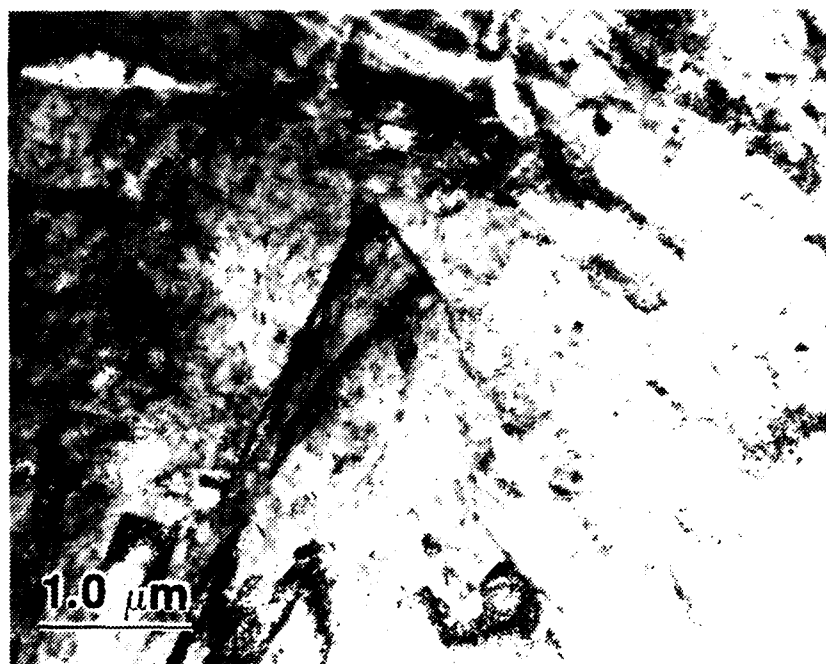


(d)

Figure 23. TEM Micrographs of the Fine HAZ from SAW and GMAW TEM Slices #3 (a and b), Respectively, from GMAW TEM Slice #4 (c and d), and from SAW TEM Slice #5 and GMAW Slice #7 (e and f), Respectively (continued)



(e)



(f)

Figure 23. TEM Micrographs of the Fine HAZ from SAW and GMAW TEM Slices #3 (a and b), Respectively, from GMAW TEM Slice #4 (c and d), and from SAW TEM Slice #5 and GMAW Slice #7 (e and f), Respectively (continued)

recovery and the formation of small subgrain boundaries from the dislocations, due to tempering, are observed (marked R). In some areas, however, a high dislocation density was observed as darker regions (marked D). Some very fine precipitates are seen (marked P) which are believed to be cementite. Many precipitates were obscured due to the high dislocation density. Figure 19(b) was included to show an autotempered martensitic structure. It was observed that many larger laths contained autotempered martensitic regions. Coarse cementite particles (marked C) are precipitated at the lath boundary and finer cementite particles are precipitated within the laths. Figure 19(c) is a bainitic region with elongated cementite particles between the ferrite laths. This structure was originally upper bainite and upon tempering the cementite between the laths was spheroidized. Some twins were also seen within the laths.

b. Weld Metal of the Last Pass

The microstructure throughout the last pass of the weld metal is represented in Figure 20 (a) through (d). Both welding processes showed a martensitic-bainitic mixture in the weld metal. In the SAW weld metal, the lath structure was poorly defined (Figure 20(a)) and seemed to be coarser and more bainitic than the GMAW weld metal. A lower dislocation density was observed in the SAW weld metal with more recovery of dislocations in some areas. There was no acicular ferrite observed in this region. Figure 20(b) shows several spherical, nonmetallic inclusions ranging in size from approximately 2 μm to 6 μm . These inclusions seem to be of an oxide nature, and may be rich

in Si or Mn [Ref. 16]. Inclusions, although present in similar numbers and sizes in both processes, were not observed in high densities. The GMAW weld metal showed a finer lath martensite structure, as seen in Figure 20(c). The second phase regions present between the martensite laths, in Figure 20(d), are probably retained austenite. The low-angle grain boundaries between the laths and areas of higher dislocation density are seen in the GMAW weld metal.

c. Weld Metal Close to Coarse HAZ

The microstructure of the weld metal close to the coarse HAZ was similar to that observed in the last pass weld metal. Figure 21(a) shows a coarse bainitic structure representative of the SAW weld metal. Signs of dislocation recovery are again seen in some localized regions. In the SAW sample, more polygonal ferrite was seen. The morphology of the GMAW weld metal consisted predominantly of lath martensite (Figure 21(b)). Twins were present in the weld metal of both samples, but the GMAW weld metal seemed to contain larger amounts. Representative bright and dark field TEM micrographs of twinned martensite observed in the GMAW weld are shown in Figure 21 (c) and (d). Retained austenite was present between the martensite or ferrite laths of both samples but appeared more frequently in the GMAW weld metal. Figure 21 (e) and (f) are bright field and dark field micrographs showing retained austenite between the laths. The dark field micrograph shows the austenite phase illuminated using a $(002)_\gamma$ diffraction spot. These two micrographs were taken in the SAW sample but are representative of both processes.

d. Coarse HAZ

The microstructures seen throughout the HAZ of the two samples were very similar, consisting of a martensitic-bainitic structure with a large amount of autotempered martensite. The SAW sample seems to be coarser, containing more bainite than the GMAW microstructure (Figure 22(a)). Figure 22(b) suggests that the GMAW sample is a finer structure containing more martensite than the SAW sample. Figure 22(c) shows the bainitic structure of the SAW heat-affected zone containing the intralath cementite particles. Figure 22(d) shows a large region of lower bainite in the GMAW heat-affected zone. Both samples revealed some retained austenite between parallel laths as well as twinned martensite within the laths.

e. Fine HAZ

The microstructures throughout the fine HAZ were similar for the two welding processes. Figure 23 (a) and (b) show the similar morphologies in the micrographs from the third TEM slices of the SAW and GMAW samples, located at approximately 1.6 mm and 1.2 mm from the fusion line, respectively. Figure 23(a) shows tempered martensite and some autotempered martensite with cementite particles precipitated between the laths at the prior austenite grain boundary. Figure 23 (c) and (d) are from the fourth TEM slice of the GMAW sample, located approximately 1.6 mm from the fusion line. Figure 23(c) shows a packet of fine parallel lath martensite which is heavily dislocated. Figure 23(d) shows a large autotempered martensite lath, containing some twins. Figure 23 (e) and (f) shows the

microstructure from the fifth SAW slice and the seventh GMAW slice (located approximately 2.7 mm and 2.8 mm, respectively, from the fusion line), which correspond to location D on the microhardness profile of Figure 10. The same autotempered martensite structure is seen in these last slices as the third slices.

V. DISCUSSION

Differences in the microstructure of the two weldments could not be readily resolved using optical and scanning electron microscopy (SEM). Transmission electron microscopy (TEM), however, allowed the differences to be observed and compared.

The microhardness profiles across the weld center and HAZ were used to identify where differences in microstructure might be expected. The subsequent microstructural characterizations tended to correlate with the microhardness profiles.

The microhardness profiles through the weld metal (Figures 9 and 10) indicated that the GMAW weld metal was generally harder than the SAW weld metal. The weld metal hardness across the region of repeated thermal cycling (Figure 11) does not, however, seem to follow the same trend of weld metal hardness. Figure 11 indicates that the weld metal of the SAW process is harder than the GMAW weld metal, but a meaningful comparison of the weld metal hardness in this region can only be performed if the effect of the subsequent thermal cycling experienced is carefully examined. This was not attempted, hence no comparison was made. The weld metal of the GMAW sample was harder and generally exhibited a finer, martensitic lath structure, while the weld metal of the SAW weldment was not as hard and consisted of a coarser, more bainitic lath structure (Figures 20 and 21). Similar microstructures were also observed by Challenger, et al. [Ref.

18] in a comparative study of SAW and GMAW processes on HY-100 steel weldments. Generally, upper bainite is considered to be less tough than tempered martensites of similar composition and strengths [Ref. 19]. Nahlor and Krahe [Ref. 19] found that in a 0.1 percent C, 1/2 Mo-B steel, decreasing the austenite grain size resulted in a decreased bainite packet size and increased toughness. This indicates that the toughness of the SAW weldment may be greater than the GMAW weldment due to the more bainitic structure of the SAW sample.

Both profiles across the weld metal center revealed the average hardness to be highest in the last pass, which was not affected by subsequent thermal cycles. The average hardness of previous passes decreased due to the tempering by subsequent passes. The minimum hardness values on the profile occurred at intersections of two heat zones which were regions which experienced a greater amount of tempering.

The microhardness across the heat-affected zones (Figure 10) of the two processes was very similar and is in agreement with the observations of similar microstructures throughout the HAZ (Figure 23). The microstructure of the HAZ in both processes was of a bainitic-martensitic duplex structure with large amounts of autotempered martensite. The GMAW weldment showed a much larger decrease in hardness at the fusion line than the SAW weldment (Figure 10). The reason for this is not quite understood, but it may be attributed to the higher heat input of the GMAW process. The

maximum hardness values of the fine HAZ were higher for the profiles across the single-pass HAZ (Figure 10) than for the profiles across the thermally cycled HAZ (Figure 11). The difference in maximum hardness can be attributed to the increased amount of tempering of the thermally cycled region which results in softening. The base metal hardness of the four profiles across the HAZ was the same.

The SEM micrographs of the weld metal of the last pass showed a refinement in microstructure as the hardness increased with the finest structure occurring at the maximum hardness location (Figures 16 and 18). The location of maximum hardness was closest to the weld crown and the location of minimum hardness was near the root of the last pass. This can be attributed to the higher cooling rate at the crown of the weld, where it is largely air cooled, whereas the bottom of the pass has a lower cooling rate.

TEM provided further analysis of the microstructures present. The GMAW weld metal seemed to contain a larger amount of retained austenite between the laths and a larger amount of twinned martensite. As ferrite forms, the carbon content of the remaining austenite is increased, which leads to the formation of twinned martensite and/or the retention of some high-carbon austenite. Twinned martensite is unlikely to form unless the carbon content of austenite exceeds about 0.2 percent [Ref. 20]. The observation of twins may indicate that inhomogeneities in carbon content existed within the austenite grains prior to transformation. Such inhomogeneities may be due to an insufficiently high temperature being reached for homogeneous dissolution

of carbides or to insufficient time spent at the high temperature. The GMAW weld metal in the as-deposited condition has a slightly higher carbon content (0.074 percent for the GMAW weld metal and 0.055 percent for the SAW weld metal), which would contribute to an increase in hardness. The SAW weld metal was observed to have more polygonal ferrite, which is coarse and has a lower carbon content than martensite, which would also contribute to the lower hardness.

In a study of HY-130 weldments, Chen, et al. [Refs. 21 and 22] observed that the fine-grained bainitic and ferritic structures were more resistant to stress corrosion cracking (SCC) than the untempered martensite and twinned martensite structures. It was also observed [Ref. 22] that the absorption of hydrogen in twinned martensite could promote SCC susceptibility and assist in brittle fracture. Since resistance to SCC is lowered by the presence of untempered and twinned martensite, the GMAW weld metal would be expected to be more susceptible to SCC due to its larger amount of twinned martensite than the SAW weldment.

The overall effect of retained austenite on properties depends mainly on the morphology. Webster [Ref. 23] states that the presence of retained austenite between martensite laths improves the fracture toughness. According to the same author, the refinement of the austenite grain size results in increases in strength and SCC resistance and decreases the fatigue crack growth rate. Thomas [Ref. 24] studied the effect of retained austenite in medium carbon alloy steels and found that thermally stable retained austenite films between

martensite laths can be beneficial for fracture toughness properties. Ritchie, et al. [Ref. 25] found that the stress corrosion crack velocity through martensite is reduced upon intersection of the retained austenite. Kim, et al. [Ref. 26] found that, in 5.5 Ni steel, austenite precipitated on the martensite laths decreases the toughness in the presence of hydrogen by increasing the severity of hydrogen embrittlement. Relating the results of previous work to this study, the retained austenite present in both weldments might be expected to increase the toughness of the weldments. The GMAW weldment might have a larger increase in toughness due to the greater amounts of interlath retained austenite present.

Several authors [Refs. 13, 15, and 16] have discussed the significant effect of fine nonmetallic inclusions on the nucleation of acicular ferrite. The low density of inclusions observed in this study might have had some effect on the absence of acicular ferrite in the GMAW and SAW weldments. The as-deposited weld metal composition has a higher amount of Mn (about 1.45 percent) and Si (about 0.38 percent) than Al (0.003 percent in the SAW or 0.014 percent in the GMAW sample). Bhatti, et al. [Ref. 15] observed that higher amounts of acicular ferrite were associated with Al-rich inclusions and lower amounts of acicular ferrite were associated with Mn-rich inclusions. This leads to the speculation that the inclusions of the two weldments under study, although not chemically analyzed, should be richer in Mn and Si rather than of an Al-rich nature. The as-deposited weld metal composition of the weldments indicates less than 0.005 percent S and an

oxygen content of 0.019 percent in the GMAW and 0.028 percent in the SAW samples. Weld metal compositions containing a higher oxygen and sulfur content generally contain a larger number of inclusions [Ref. 18]. The low density of inclusions in the SAW and GMAW weld metals can be a result of the low sulfur and oxygen contents.

It is seen that the differences in microstructure of the SAW and GMAW weldments tended to correlate with the microhardness profiles of the center weld metal and across the HAZ. The observations made and conclusions drawn were largely in agreement with studies by previous authors.

VI. SUMMARY

The effect of welding processes, gas-metal-arc (GMAW) and submerged-arc (SAW), on the microstructure of HY-130 steel multi-pass weldments was studied and compared. Microhardness measurements, optical, scanning, and transmission electron microscopy were used to characterize the microstructures. The microhardness profiles of the GMAW and SAW weldments showed the same general trend with the microstructure throughout the HAZ of a single-pass region showing no significant differences. The major microstructural and microhardness differences between the two processes occurred in the weld metal. The GMAW weld metal consisted of a more predominant martensitic structure with a finer lath morphology than the SAW weld metal. The GMAW weld metal also contained more twinned martensite and more retained austenite. The SAW weld metal has a less-defined lath and more-bainitic structure. The last-pass weld metal of the GMAW sample was approximately 40 VHN harder than the SAW sample, so the GMAW weldment may be expected to have a higher strength. A general recommendation of one welding process over the other cannot, however, be made based on the present study because the selection of welding process depends on a large number of other factors.

LIST OF REFERENCES

1. Flax, R. W., Keith, R. E., and Randall, M. D., *Welding the HY Steels*, ASTM Special Technical Publication 494, pp. 1-25, 1971.
2. Palko, W. A., Bryne, J. P., and Zanis, C. A., "Processing of HY-130 Steel Castings," *American Foundrymen's Society Transactions*, v. 84, pp. 193-202, 1976.
3. David Taylor Naval Ship Research and Development Center Report SME-85/109, *Welding of Thin Section HY-130 Steel Progress Report*, by R. J. Wong, pp. 1-38, January 1986.
4. Grong, O., and Matlock, D. K., "Microstructural Development in Mild and Low-Alloy Steel Weld Metals," *International Metals Review*, v. 31, number 1, pp. 27-45, 1986.
5. British Steel Corporation Research Organization, *Weld Metal Microstructure—A State of the Art Review*, by R. C. Cochrane, pp. 1-8, October 1982.
6. Krauss, G., *Principles of Heat Treatment of Steel*, pp. 43-83, American Society for Metals, 1980.
7. Thompson, S. W., Colvin, D. J., and Krauss, G., "On the Bainitic Structure Formed in a Modified A710 Steel," *Metallurgical*, v. 22, pp. 1069-1074, 12 March 1988.
8. Easterling, K., *Introduction to the Physical Metallurgy of Welding*, Butterworths, pp. 150-153, 1983.
9. Therrien, A. E., *Characterization of Submerged-Arc and Gas-Metal-Arc Weldments in HY-100 Steel*, Master's Thesis, Naval Postgraduate School, Monterey, California, December 1983.
10. *Metals Handbook*, 9th ed., v. 6, pp. 114-181, American Society for Metals, 1983.
11. Challenger, K. D., Brucker, R. B., Elger, W. M., and Sorek, M. J., "Microstructure-Thermal History Correlations for HY-130 Thick Section Weldments," *Welding Journal*, v. 63 (8), pp. 254s-262s, 1984.

12. Abson, D. J., and Dolby, R. E., "Microstructural Transformations in Steel Weld Metals—A Reappraisal," *Welding Institute Research Bulletin* 19, pp. 20-206, July 1978.
13. Farrar, R. A., and Harrison, P. L., "Review Acicular Ferrite in Carbon-Manganese Weld Metals: An Overview," *Journal of Materials Science*, v. 22, pp. 3812-3820, April 1987.
14. Glover, A. G., McGrath, J. T., Tinkler, M. J., and Weatherly, G. C., "The Influence of Cooling Rate and Composition on Weld Metal Microstructures in a C/Mn and a HSLA Steel," *Welding Research Supplement*, v. 55, pp. 267s-273s, 1976.
15. Bhatti, A. R., Saggese, M. E., Hawkins, D. N., Whiteman, J. A., and Golding, M. S., "Analysis of Inclusions in Submerged Arc Welds in Microalloyed Steels," *Welding Journal*, v. 63 (7), pp. 224s-230s, July 1984.
16. Lui, S., and Olson, D. L., "The Role of Inclusions in Controlling HSLA Steel Weld Microstructures," *Welding Research Supplement*, v. 65, pp. 139s-149s, June 1986.
17. Ricks, R. A., Barritte, G. S., and Howell, P. R., "The Influence of Second Phase Particles on Diffusional Phase Transformations in Steels," *Proceedings of International Conference on Solid State Phase Transformations*, pp. 463-468, 1981.
18. Deb, P., Challenger, K. D., and Therrien, A. E., "Structure-Property Correlation of Submerged-Arc and Gas-Metal-Arc Weldments in HY-100 Steel," *Metallurgical Transactions*, v. 18A, pp. 987-997, June 1987.
19. Naylor, J. P., and Krahe, P. R., "The Effect of the Bainite Packet Size on Toughness," *Metallurgical Transactions*, v. 5, pp. 1699-1701, July 1974.
20. Speich, G. R., and Leslie, W. C., "Tempering of Steel," *Metallurgical Transactions*, v. 3, pp. 1043-1054, May 1972.
21. Chen, C., Thompson, A. W., and Bernstein, I. M., "The Correlation of Microstructure and Stress Corrosion Fracture of HY-130 Steel Weldments," *Metallurgical Transactions*, v. 11A, pp. 1723-1730, October 1980.

22. Chen, C., Thompson, A. W., and Bernstein, I. M., "Microstructure and Stress Corrosion Cracking of HY-130 Steel Weldments," paper presented at the Bolton Landing Conference, 5th, Schenectady, New York, 1979.
23. Webster, D., "Development of a High Strength Stainless Steel with Improved Toughness and Ductility," *Metallurgical Transactions*, v. 2, pp. 2097-2114, August 1971.
24. Thomas, G., "Retained Austenite and Tempered Martensite Embrittlement," *Metallurgical Transactions*, v. 9A, pp. 439-450 March 1978.
25. Ritchie, R. O., Castro Cedeno, M. H., Zackay, V. F., and Parker, E. R., "Effects of Silicon Additions and Retained Austenite on Stress Corrosion Cracking in Ultrahigh Strength Steels," *Metallurgical Transactions*, v. 9A, pp. 35-52, January 1978.
26. Kim, Y. H., Kim, H. J., and Morris, J. W., Jr., "The Influence of Precipitated Austenite on Hydrogen Embrittlement in 5.5 Ni Steel," *Metallurgical Transactions*, v. 17A, pp. 1157-1164, July 1986.

INITIAL DISTRIBUTION LIST

| | <u>No. Copies</u> |
|--|-------------------|
| 1. Defense Technical Information Center Cameron Station Alexandria, VA 22304-6145 | 2 |
| 2. Library, Code 0142 Naval Postgraduate School Monterey, CA 93943-5002 | 2 |
| 3. Department Chairman, Code 69Hy Department of Mechanical Engineering Naval Postgraduate School Monterey, CA 93943-5000 | 1 |
| 4. Dr. Saeed Saboury P. O. Box 51922 Pacific Grove, CA 93950 | 2 |
| 5. Dr. J. M. B. Losz, Code 69Lo Department of Mechanical Engineering Naval Postgraduate School Monterey, CA 93943-5000 | 2 |
| 6. Professor T. R. McNelley, code 69Mc Department of Mechanical Engineering Naval Postgraduate School Monterey, CA 93943-5000 | 1 |
| 7. Mr. Paul W. Holsberg, Code 2815 David Taylor Naval Ship Research and Development Center Annapolis, MD 21402-5067 | 1 |
| 8. Mr. G. L. Franke, Code 2815 David Taylor Naval Ship Research and Development Center Annapolis, MD 21402-5067 | 1 |

- | | | |
|-----|--|---|
| 9. | Mr. R. J. Wong, Code 2815 David Taylor Naval Ship Research and Development Center Annapolis, MD 21402-5067 | 1 |
| 10. | Capt. T. M. McNutt, CF 13 Paula Crescent Nepean, Ontario, Canada K2H 8Y8 | 3 |
| 11. | Anti-Armour Light Armoured Vehicle Project National Defence Headquarters Major-General George R. Pearks Building Ottawa, Ontario, Canada K1A 0K2 | 1 |
| 12. | Director Personnel Education and Development National Defence Headquarters Major-General George R. Pearks Building Ottawa, Ontario, Canada K1A 0K2 | 1 |
| 13. | Director General Land Engineering and Maintenance National Defence Headquarters Major-General George R. Pearks Building Ottawa, Ontario, Canada K1A 0K2 | 1 |